SLAC-PUB-516
(EXPI)

DETAILED STUDY OF THE ELECTRON-PHONON INTERACTION IN ALKALI HALIDES*

PART II

TRANSMISSION SECONDARY EMISSION FROM ALKALI HALIDES

J. Llacer and E. L. Garwin

Stanford Linear Accelerator Center
Stanford University, Stanford, California

* Work supported by the U. S. Atomic Energy Commission.

ABSTRACT

The phenomenon of secondary emission from alkali halides is studied in transmission. This allows the variation of one more parameter (thickness) than in conventional reflection studies. An empirical method based on published results of scattering by thin foils is used to determine the spatial dependence of the internal electron excitation function. The results of the Monte Carlo calculations presented in the previous paper (Part I) are used to generate a mathematical model of secondary emission. Measurements of pulsed secondary yield and of energy distribtuion of secondary electrons from uncharged films of CsI, KCl, NaF, and LiF are carried out at various film thicknesses and primary energies. By matching one single experimental point to the mathematical model, complete theoretical curves of yield for each material are generated. The results show that the spatial dependence of the excitation function taken together with the secondary escape results of Part I are sufficient to account for the variations of yield of different materials as a function of thickness and primary energy. An absorption attributed to d-like conduction bands is experimentally observed in KCl. The energy dependence of the internal excitation function is obtained and it is also shown that it is incorrect to characterize the probability of escape of all internal secondaries by a single exponential. The implications and shortcomings of the experiments are discussed.

I. INTRODUCTION

The subject of Secondary Electron Emission has received considerable attention since it was first observed in 1902 by Austin and Starke.[1] Excellent review articles have appeared in the literature, principally those by McKay,[2] Bruining,[3] Kollath,[4] and Dekker,[5] covering the great wealth of experimental information as well as the somewhat limited theoretical understanding until 1958. Since that date, contributions by Kanter[6,7,8] and by Kanter and Sternglass[9] have considerably improved the understanding of some important concepts. Relatively little fundamental work has been reported on the subject for the last few years.

It has been traditional to divide the problem of secondary emission into two parts: (a) the loss of energy suffered by the primary electrons penetrating a solid, with the consequent excitation of electrons to energies above the vacuum level of the material, and (b) the energy loss mechanisms of conduction electrons, determining the fraction of excited electrons which are actually able to leave the solid.

As observed by Dekker,[5] the separation into two problems may not be very meaningful for the case of metals and narrow gap ($\approx$ 1 eV) semiconductors. In the case of insulators, however, the separation is considerably more reasonable. Electrons excited to energies between the conduction band energy and the conduction band plus the energy of the first excitonic absorption peak cannot suffer further inelastic collisions with valence band electrons. Thus it appears plausible to define a generation function F, as a result of part (a) of the problem, giving details as to the excitation of electrons by the primary beam of electrons. Problem (b) is then concerned with calculating escape probabilities for those electrons.

It is the purpose of this paper to report: (1) an empirical method for finding the spatial dependence of the excitation function F, (2) a mathematical model for the escape of the excited electrons based on the results of the Monte Carlo calculations of the previous paper (Part I), (3) the techniques and results of measuring secondary emission coefficients and energy distributions of secondaries from alkali halide films and (4) calculations with the mathematical model and comparisons to experimental results. Apart from elucidating the secondary emission process in alkali halides, the work reported confirms, to a large extent, the quantitative results obtained by the application of perturbation theory to the electron-phonon interaction in those materials.

The investigation has been carried out in transmission, i.e., the primary electrons strike the secondary emitting film at one face and the secondaries and transmitted primaries are collected from the other face. The advantage of this method is that the thickness of the alkali halide emitter can be changed giving one more important parameter for the comparison of experiments with theory.

II. THE SPATIAL DEPENDENCE OF THE EXCITATION FUNCTION

When primary electrons strike a target, there exists a function $-(dE/dx)$ corresponding to the average energy lost by a primary electron per unit length. Usually the beam strikes the surface perpendicularly and the x direction is taken to be the same as the beam, or forward direction. If the function $-(dE/dx)$ is obtained in some manner, the x dependence of the excitation function becomes available, as Kanter[7] has experimentally proven their proportionality.

Assuming that the excited electrons have an isotropic distribution of velocities, the production of internal secondaries between energies $\mathcal{E}_0$ and $\mathcal{E}_0 + d\mathcal{E}_0$ in a slab

of thickness dx at x is then given by

$$F(x, \mathcal{E}_0) = \left(- \frac{dE}{dx} (x) \right) G(\mathcal{E}_0)\, d\mathcal{E}_0 dx \quad , \tag{1}$$

where $G(\mathcal{E}_0)$ is a function giving the average number of electrons generated isotropically with energies between $\mathcal{E}_0$ and $(\mathcal{E}_0 + d\mathcal{E}_0)$ per unit of energy loss suffered by the primary beam.

The review articles[2-5] give an account of the work done until 1958 towards the evaluation of $-(dE/dx)$. In 1964 Jahrreiss[10] modified Sternglass' theory of secondary emission[11] to make it applicable to transmission and more recently Anderson, Laponsky, Peria, et al.,[12] have obtained an expression for $-(dE/dx)$ which appears to fit quite well experimental results for MgO. However, the existence of Kanter's detailed measurements of electron scattering by thin foils[6] has suggested an empirical method for finding $-(dE/dx)$ which is not limited by theoretical complexities, but which has some computational limitations. In some cases these limitations can be overcome satisfactorily. The approach consists in differentiating with respect to thickness Kanter's results for transmission through thin foils.

Initial work was carried out by Young[13] who measured the fraction of transmitted current versus energy of the incoming electrons for several thicknesses of Al_2O_3 film. He defined a practical range for the electrons as the extrapolation to zero transmission of the linear part of the transmission versus energy curves obtained experimentally.

Later, Kanter measured the fraction of transmitted electrons, η_t, versus initial energy for various materials and thicknesses, as well as average and most probable exit energies (E_a and E_w respectively), and average and most probable angle of scattering (θ_a and θ_w). He found that by defining the energy of the incoming primary electron, E_p, in units of a critical energy, E_c, corresponding to the initial energy of an electron with practical range equal to the thickness of the film under investigation, all the transmission data for different

materials could be presented in a compact form in one graph. Likewise, for the energy and angle data.

Consider then dividing a film into a number of slabs and computing successively the contribution to energy loss by each slab. No backscattering is assumed at first. For a given thickness of remaining slabs, E_c is found by a convenient form of the Energy-Range relation

$$E_c = \left(\frac{R^{\mu g/cm^2}}{13.5}\right)^{0.77} \quad (keV) \tag{2}$$

obtained empirically from the results presented by Kanter. The fraction of transmitted electrons, η_t, as a function of reduced initial energy E_p/E_c, for films of thickness $\geq 15\ \mu g/cm^2$, as given by Fig. 4 of Ref. 6, can be represented very well in the energy range of $1 \leq E_p/E_c \leq 5$ by the expression

$$\eta_t = \left[1 - \exp\left(-\frac{\gamma - 1}{\gamma'}\right)\right] \tag{3}$$

where $\gamma = E_p/E_c$ and γ' is a linear function of atomic number Z:

$$\gamma' = .45 + .025\ Z \quad . \tag{4}$$

The fractional average energy E_a/E_p of transmitted electrons as a function of γ, as given by Fig. 8 of Ref. 6, is fitted again quite well by an exponential in the region $1 \leq \gamma \lesssim 6$.

$$E_a/E_p = .45\left[1 - \exp\left(-\frac{\gamma - 1}{1.33}\right)\right] + .4 \tag{5}$$

For $\gamma > 6$, the above expression approaches .85. This cannot be a good representation at large γ, in which case E_a/E_p should approach almost unity. Since Kanter's results are not extended to such regions, the calculation to be presented will be in error whenever $\gamma \gtrsim 6$.

By using the above expressions, it is possible to write a simple computer program which will find the average energy loss suffered by a beam of electrons of primary energy E_p, with a density of 1 electron/cm^2. For the purpose of illustration consider a film of Al, with a thickness of 100 μg/cm^2, divided into 10 slabs. A beam of 6 keV electrons enters normally at x = 0. The energy loss in traversing the 10 slabs is found to be 5.1 keV. Next, we assume that the last (at exit side) slab does not exist. The energy lost by the beam is 4.77 keV, giving $-(dE/dx) = (5.1-4.77)/10 = .033$ keV $-(\mu g/cm^2)^{-1}$. The same procedure is repeated until all the slabs have been eliminated. Figure 1 shows the energy lost by a 6 keV electron from these initial calculations. The inadequancy of Eq. (5) at the higher values of γ becomes quite evident in Fig. 1: For x approaching zero, the energy loss should go to zero. A correction is proposed in which a linearly increasing energy loss is suffered by the electrons up to a thickness such that $-(dE/dx)$, as calculated above, matches the slope of the linear loss. This correction is also shown in Fig. 1. If on physical grounds one excludes the possibility of discontinuities and of more than one maximum in $-(dE/dx)$, the linear loss approximation is the only possible solution for these calculations.

The corrections for backscattering can be applied at this point. The energy loss computed above includes the energy not transmitted because it is backscattered by the film. This backscattered energy does not contribute (to first order) to the generation of electrons. A correction is, therefore, necessary. The first difficulty is in trying to specify a backscattering coefficient η for thin films as a function of energy of the incident electron. Halliday and Sternglass[14] show η versus atomic number for bulk materials. More information is available in a paper by Gomoyunova and Letunov.[15] The former work also shows that the value of η for bulk materials holds for thin films, as long as the incident electrons are

of an energy $E_p \leq 2\ E_c$ for the thickness of the film. For higher E_p, the only available data are for a 500 Å Al film, given by Kanter.[8] As a reasonable approximation, one can form a function $\eta\left(E_p/E_c\right)$ which is proportional to the one for Al. The proportionality constant is then found by requiring that at low E_p, $\eta = \eta_{bulk}$. This function can be represented by

$$\eta = \eta_{bulk} \text{ for } \gamma \leq 2$$

$$= \eta_{bulk} \exp\left(-\frac{\gamma - 2}{3.75}\right) \text{ for } \gamma \geq 2 \qquad (6)$$

which fits Fig. 2 of Ref. 8 quite well up to $\gamma \approx 8$.

The procedure for the calculation is similar to the previous one. Consider first the 10th slab. The primary electron which started at 6 keV, reaches the 10th slab with an average energy of $\approx .89$ keV. The average angle of arrival is not zero, but this will be disregarded given the approximate nature of the correction. Since the average energy of backscattered electrons is approximately one half the energy of the bombarding electrons,[8] the energy backscattered by the last slab can be computed. Next one takes the 9th and 10th slabs and the procedure is repeated until the total energy backscattered is found. The correction to the total energy loss up to the slab at x_i is equal to total backscatter energy minus the energy backscattered by the material at $x > x_i$. The backscattering correction is also shown in Fig. 1, as well as the values of $-(dE/dx)$. It can be seen that the backscattering correction is not of great significance in this particular case; however, for higher Z materials the correction is more substantial.

The practical films used at the Stanford Linear Accelerator Center for the study of transmission secondary emission consist of a 1000 Å Al_2O_3 supporting film, a 500 Å film of Al and finally an evaporated film of an alkali halide. For

the purposes of this investigation, the 1000 Å Al_2O_3 and the 500 Å Al films will be considered as a substrate. The energy loss suffered by the primary electrons in traversing the substrate is certainly not negligible and its presence cannot be neglected.

Since the average Z of Al_2O_3 is not very far from that of Al, one can use Kanter's transmission measurements[6] to find the average number of electrons transmitted by the substrate, their average energy and their average angle for a normally incident beam. The results are then used as initial values for the computation of $-(dE/dx)$ in the alkali halide film. The angular information is used to determine an effective thickness $\tau' = (\tau/\cos\theta_{av})$ where τ is the true film thickness of the alkali halide and θ_{av} is the average angle of the incoming electrons. The energy loss and backscattering corrections are computed for a film of thickness τ', but the derivative $-(dE/dx)$ is taken in the forward direction, so that the final result is given in keV $-(\mu g/cm^2)^{-1}$ in the direction normal to the film surface. This method of calculation is approximate, and it is only appropriate if the electrons transmitted by the substrate have an angular distribution which is independent of their energy distribution. There does not seem to be any available information to substantiate such independence. Computations for two alkali halides, with quite different Z are shown in Figs. 2 and 3. Both computations have been carried out with 100 slabs covering the full thickness τ. Results with (solid line) and without (dashed line) the linear loss correction are shown. The linear loss correction can only be computed for thicknesses above a certain minimum. In a practical problem with τ less than such a minimum the computation of the correction will be carried out for a thicker film.

Results obtained for MgO by the above method have been compared to those of Anderson et al.,[12] for the same material and were found to agree

in the general shape and magnitude of - (dE/dx), although they are substantially different in detail. It is felt that the empirical approach used here provides a quantitative basis for use in the following steps, with a well-defined (and physically realistic) method for handling the available experimental data.

III. MATHEMATICAL MODEL

The escape probability of internal secondary electrons as governed by the electron-phonon interaction has been studied in Part I of this work. For electrons generated isotropically, the escape probability was found to be approximately exponential in character, particularly for films above 250 Å in thickness, so that a characteristic escape length $L_s(\mathcal{E}_0)$ dependent on the initial energy of the electron $\mathcal{E}_0$ and on material can be defined. Likewise, a constant $P_0(\mathcal{E}_0)$ corresponding to the probability of escape of electrons generated isotropically at the film exit surface was given.

From the excitation function $F(x,\mathcal{E}_0)$ given by Eq. (1) and assuming that the escape of secondaries is not governed by any mechanism beyond the electron-phonon interaction, the secondary yield δ should be obtainable from an expression

$$\delta = \int_x \int_{\mathcal{E}_0} G(\mathcal{E}_0) \left(-\frac{dE}{dx}(x)\right) P_0(\mathcal{E}_0) \exp\left[-\frac{\tau - x}{L_s(\mathcal{E}_0)}\right] d\mathcal{E}_0 dx \qquad (7)$$

where the integral over x runs over the film thickness and the integral over $\mathcal{E}_0$ should cover the range of energies of internally generated electrons. For the present calculations made at discrete values of x and $\mathcal{E}_0$, Eq. (7) is approximated by

$$\delta = \sum_{\mathcal{E}_{0j}} G(\mathcal{E}_{0j}) P_0(\mathcal{E}_{0j}) \left\{ \sum_{x_i} \left(-\frac{dE}{dx}(x_i)\right) \exp\left[-\frac{\tau - x_i}{L_s(\mathcal{E}_{0j})}\right] \Delta x \right\} \Delta \mathcal{E}_{0j} \ . \qquad (8)$$

For a given $\mathcal{E}_{0j}$ the summation over x_i is carried out by using the results of Section II of this paper for $-(dE/dx)$ and the values of L_s from Table 1 of Part I. Then, the expression between brackets in Eq. (8) is calculated from theory, and given as a function $S(\mathcal{E}_{0j})$.

Each term of the summation over $\mathcal{E}_{0j}$ can be described as the contribution to δ by electrons generated with an energy spread $\Delta\mathcal{E}_{0j}$ about $\mathcal{E}_{0j}$. When these electrons reach the exit surface they do so with energies which are in general below $\mathcal{E}_{0j}$ and a spread larger than $\Delta\mathcal{E}_{0j}$.

In order to relate each term of Eq. (8) to an experimentally determined secondary energy distribution $N(\mathcal{E}_j)$, a simplifying approximation has been made. It consists in assuming that electrons generated with energy $\mathcal{E}_{0j}$ suffer an average energy loss $(\mathcal{E}_{0j} - \mathcal{E}_j)$ in travelling to the surface and each term in the summation over $\mathcal{E}_{0j}$ of Eq. (8) can be related to the corresponding value of $N(\mathcal{E}_j)$. With $N(\mathcal{E}_j)$ normalized to unity area, we have

$$N(\mathcal{E}_j)\ \delta = G(\mathcal{E}_{0j})\ P_0\ (\mathcal{E}_{0j})\ S\ (\mathcal{E}_{0j}) \tag{9}$$

Both $P_0\ (\mathcal{E}_{0j})$ and $S\ (\mathcal{E}_{0j})$ are obtained theoretically, while $N\ (\mathcal{E}_j)$ is obtained experimentally as is δ for a chosen material, primary energy, and thickness. Then in this model, $G\ (\mathcal{E}_{0j})$ can be obtained from only one measurement, and is unique for a given material, i.e., it is independent of thickness and primary energy. Substituting the calculated values of $G\ (\mathcal{E}_{0j})$ into Eq. (8), gives the secondary yield for all thicknesses and primary energies for a given material. Comparison with complete experimental results then constitutes a test for the correctness of the calculations of $-(dE/dx)$ (except for a multiplicative constant) and of L_s.

The relationship between $\mathcal{E}_{0j}$ and $\mathcal{E}_j$ is estimated approximately for the four alkali halides investigated from the results shown in Figs. 9 to 12 in Part I. Assuming an energy loss of the form $(a\,x + b)$ from the figures, a value of $-(dE/dx)$ essentially constant at the thickness and E_p chosen for the measurement, and using the computed values of L_s, the average energy loss is

$$\mathcal{E}_{0j} - \mathcal{E}_j \simeq \frac{\int_{x'=0}^{\tau} (a\,x' + b) \exp\left[-\frac{x'}{L_s(\mathcal{E}_{0j})}\right] dx'}{\int_{x'=0}^{\tau} \exp\left[-\frac{x'}{L_s(\mathcal{E}_{0j})}\right] dx'} \tag{10}$$

where x' corresponds to $(\tau - x)$ in previous expressions.

IV. MEASUREMENTS OF TRANSMISSION SECONDARY YIELD

Extensive measurements of secondary emission in reflection have been carried out in metals, semiconductors and insulators. The review articles[2,3,4,5] give a comprehensive account of the most important results obtained to 1958. The work of Jahrreiss[10] contains an extensive updating to 1964 of reflection and transmission measurements. In 1965, a comprehensive study of reflection secondary emission in all the alkali halides was reported by Gomoyunova and Letunov,[16] and in 1966 Edgecumbe and Garwin[17,18] reported measurements in transmission for CsI and KCl.

It is well known that secondary emission from insulators results in charging of the emitter. This charging can have a considerable effect on the secondary emission coefficient δ, as found by Jacobs[19] in normal density films of MgO measured in reflection. For alkali halide films, charging effects are strong in low density deposits, as reported initially for KCl by Goetze, Boerio

and Green,[20] but very little information is to be found in the literature regarding enhancement of secondary yield in normal density films, or of the energy distribution of emitted secondaries.

The requirements for the measurement of secondary yield, δ, in insulators are well known. In order to avoid charging, a pulsed measurement is needed with as few electrons per pulse as possible. The system must be designed to minimize systematic errors due to scattering and to undesired secondary emission from electrodes in the tube. The tube assembly shown schematically in Fig. 4 and the electronic set up of Fig. 5, fulfill these requirements. In Fig. 4, the simple Pierce design of electron gun consists of a filament (1), a focusing and control electrode (2), and an anode (3) with an opening of .8 cm diameter operating at ground potential. The filament is supplied from a floating dc power supply. The control electrode is supplied by a floating voltage source of up to -1000 V. D. C. with respect to the filament. The accelerating potential is applied to the filament and the current and focusing are controlled by filament temperature and control electrode-to-filament potential.

The electrons leaving the anode opening find a 3-plate collimator (4). The drift space in the tube is magnetically shielded by a nickel tube (5). The primary beam then enters an almost fully enclosed system, consisting of the next four electrodes, through an aperture of 1.6 cm diameter on top of electrode (6). Electrode (6) which operates at - 90 volts, consists of a grid for the suppression of secondary emission from the entrance side of the dynode (7) and a Faraday cup for the collection of electrons backscattered from the dynode. (No attempt has been made to eliminate secondary emission from the walls of the cup due to backscattered primaries because it does not affect the measurements.) This entire suppressor structure is designated G0. The dynode (7) consists of an Al support ring of 5 cm diameter and approximately 4 mm thickness with an opening of 2.5 cm diameter. A 1000Å film of Al_2O_3 obtained by

anodic oxidation and etching of very pure Al foil[21] is glued to the support, and 500Å of Al are evaporated onto it to supply electrical contact to the alkali halide.[22] The dynode is easily mounted onto its holder in the tube. The dynode is designated D. It is operated at ground potential.

The collector assembly is formed by a collector (9), designated C, and a suppressor grid (8) designated G1. The collector assembly is again a Faraday cup with an aperature of 4.5 cm diameter placed at a distance of .9 cm from the dynode, and is designed to prevent the majority of high energy electrons backscattered by the collector from reaching the dynode. The grid G1 suppresses secondary emission from the collector and/or from the dynode, depending on the measurement.

The anode (3), the collimators, and the cage (6) are made of stainless steel. The collector and its diaphragm are of aluminum. The grids are 97% open Ni, 20 lines per inch. Ceramic insulators are used throughout.

With the collector assembly moved out of position, the dynode area is exposed to a boat directly underneath containing previously melted halide salts. The dynode to boat distance is approximately 18 cm. A water-cooled quartz-crystal thickness monitor is situated at the same distance from the boat.

The system is enclosed in a Viton-sealed glass belljar vacuum system. Initial rough pumping to about 130 torr is provided by a venturi-type pump driven by oil—free compressed air. Then two Vac-Sorb pumps reduce the pressure to 5 millitorr, at which point a 400 ℓ/sec ion pump takes over. With the system vented exclusively to dry N_2, it is possible to cycle to about 5×10^{-7} torr several times a day without warming up the roughing pumps. A pressure of 2×10^{-8} torr is reached in about 6 hours.

Two standard measurements are normally performed: (1) Measurement of transmission yield, δ_t, in which one is interested in finding the total number of electrons leaving the dynode, regardless of energy. (2) Measurement of transmission coefficient, η_t, in which one wants to suppress secondary emission from the dynode, and measure only the energetic electrons transmitted.

Fig. 5 shows the circuits for carrying out both measurements in dc or pulsed modes. Bias for the four electrodes is supplied by floating batteries through 8.2 MΩ resistors. For dc measurements, the currents I_C and I_{G1} are added and measured by a floating battery-operated electrometer. This total current, I_{C+G1}, is then added to $I_{G0} + I_D$ and measured by a second electrometer as the primary current. The transmission gain δ_t, transmission coefficient η_t, and gain δ are then given by

$$\delta_t = \frac{-I_{C+G1}}{.97\, I_p} \qquad \text{for} \qquad \begin{matrix} V_C = +90\ V \\ V_{G1} = +45\ V \end{matrix} \tag{11}$$

$$\eta_t = \frac{-I_{C+G1}}{.97\, I_p} \qquad \text{for} \qquad \begin{matrix} V_C = 0\ V \\ V_{G1} = -45\ V \end{matrix} \tag{12}$$

$$\delta = \delta_t - \eta_t \tag{13}$$

The factor of .97 in Eq. (11) takes into account the fact that approximately 3% of primaries are intercepted by the suppressor grid of G0.

For pulsed measurements, the control electrode of the electron gun is biased beyond cutoff, and single 5 μsec pulse of sufficient amplitude to turn the beam on (usually + 30 to 40 volts) is applied to the control electrode from a Tektronix 161 pulse generator. Field effect transistor preamplifiers operating as charge integrators with a single decay time constant of 50 μsec pick up

the pulses from $I_{G0 + D}$ and $I_{C + G1}$. The sum of the two signals is $-I_p$, the primary current. Both $I_{C + G1}$ and I_p are further amplified and integrated and differentiated with a time constant of 10 μsec to obtain nearly optimum simple filtering. Those signals are then displayed simultaneously on a storage oscilloscope.

A series of careful tests has been carried out in order to estimate the magnitudes of systematic and random errors introduced into the measurement of secondary yield δ. In the worst case, a very high gain alkali halide, the true value of δ can be anywhere between the measured value $\delta_{meas.}$, and $(0.99\delta_{meas.} - 0.4\eta_t - 0.01)$. Most of this possible systematic error is due to secondary emission from transmitted primaries scattered back to the dynode surface from the collector cage.

The maximum random error in the dc measurement of δ is estimated to be $\pm 3\%$. The estimated errors for pulsed measurements is estimated at $\pm 3\%$, with pulses of 2 to 5×10^{-14} Coulombs. This error is due in part to amplifier noise and in part to inaccuracy in reading the oscilloscope traces.

Several measurements with CsI, KCl, and NaF showed that the effects on secondary yield of evaporation rate and system pressure are small at pressures ranging between 10^{-5} and 2×10^{-8} torr and rates between 1 and 10 Å/sec. All evaporations for the measurements reported were carried out at about 2×10^{-8} torr and at rates near 5 Å/sec. The vacuum system was vented to dry nitrogen, with relative humidity in the enclosing plastic box of less than 1.5%. Materials used had a purity of at least 99.9% and Mo or Ta boats previously fired in vacuum have been used for the evaporation.

For each material, six films with thickness of approximately 125, 250, 375, 500, 750, and 1000 Å were measured at room temperature. Fig. 6 through 9 show the measured secondary emission transmission yields for

CsI, KCl, NaF, and LiF. (The vertical scale has been magnified by a factor of two in the case of LiF.) The vertical error bars correspond to a sum of systematic and random errors for the worst cases. The solid curves are theoretical results discussed in Section VI. Comparisons between pulsed and dc measurements indicate no dc yield enhancement for CsI, KCl, or LiF. Yield enhancement is clearly shown in NaF. For example, a 385 Å film bombarded at 8 keV initially showed a pulsed δ of about 5. Under dc conditions, δ increased to 6 measured either by dc methods or by a pulsed beam superimposed on the steady current. Ten minutes after beam turn off, pulsed yield was down to 5.6, later decaying to 5.3. The process was reproducible. Some evidence of dissociation of NaF during evaporation has been found, as will be discussed below. If the NaF films contain more imperfections than those of the other salts, it is possible that low energy electrons (bottom of the conduction band) are in fact prevented from neutralizing the trapped holes left by emitted secondaries. This would result in a build-up of internal field and an enhancement of secondary emission in NaF films.

V. MEASUREMENT OF ENERGY DISTRIBUTION

The measurement of the energy distribution of secondary electrons from insulators is made difficult by the possibility of charge accumulation at or near the exit surface. By using low primary currents, Geyer[23] was able to make some measurements of energy distribution for different thicknesses of NaCl, in reflection. Petzel[24] published curves of energy distribution for single crystals of KCl with a correction for contact potential. Comparison of the two results shows a definite discrepancy in the peak of the energy distribution

from less than .05 eV (Geyer) to ≈1.5 eV (Petzel) which makes the results somewhat doubtful, as the two materials should not be very different. These difficulties point out the need for a system capable of measuring contact potential differences (cpd) simultaneously with making retarding potential measurements. In addition, for the purposes of the present investigation, energy distribution measurements should be carried out on films known to be uncharged.

For the measurements reported here, a tube with planar geometry and a Kelvin probe in the collector plane was used because it has, compared to transverse electron beam or second probing electron gun systems, these advantages: Possibility of very good sensitivity without critical alignment problems; ease of calibration at different collector-to-dynode spacings; small well defined area of cpd measurement, undisturbed charge state of the film during cpd measurement, and ease of recording results.

Figure 10 shows schematically a physical set up for the measurement of potential difference (pd) by a Kelvin probe. A metallic substrate holding a thickness x_1 of material with a free charge distribution $\rho(x)$ is connected to ground through a battery V_D which includes the contact potential difference (cpd) between the metallic substrate A and the vibrating capacitor plate B. The latter is connected to ground via R_L in parallel with C_L.

By comparing the induced charge Q_B at plate B with and without the charge distribution $\rho(x)$ one can show that as long as $x_1 << d$, Q_B will be proportional to the true potential at x_1, regardless of the form of $\rho(x)$.

When the plate vibrates in such a way that the capacitance C is approximately equal to $C_0 + C_1 \cos \omega t$, $C_1 << C_0$, the differential equation for $V_1(t)$ is

$$C \frac{dV_S}{dt} - C \frac{dV_1}{dt} + V_S \frac{dC}{dt} - V_1 \frac{dC}{dt} = C_L \frac{dV_1}{dt} + \frac{V_1}{R_L} , \qquad (14)$$

where V_s is the potential with respect to ground at the surface x_1.

Changing Eq. (14) to time independent coefficients by taking $C = C_0$ in the first two terms (i.e., $C_1 << C_0$), and leaving out the fourth term ($V_s >> V_1$), the steady state ac part of the solution is

$$V_1(t) = \frac{-V_S \omega C_1}{C_0 + C_L} \quad \frac{\sin(\omega t - \psi)}{\left[\left(\frac{1}{\tau}\right)^2 + \omega^2\right]^{1/2}} \tag{15}$$

where $\tau = R_L(C_0 + C_L)$.

Notice that for $\omega\tau << 1$, the phase angle ψ approaches zero so that the signal voltage is practically in quadrature with the displacement from equlibrium of the vibrating plate. This is important for the purpose of making cpd measurements when the primary beam is on. As will be seen from the description of the physical set up, the vibrating probe picks up an ac current from the electrons present between dynode and collector. The magnitude of this current can be orders of magnitude larger than the desired signal at the probe. It is the near quadrature of the two signals that allows a proper separation by the use of a synchronous detector. Anderson, Laponsky, Peria et al.,[12] observed this difficulty in their measurements of surface potential but did not resort to the near quadrature elimination, resulting in a considerable limitation in their measurements.

Figure 11 shows a schematic drawing of the tube containing the Kelvin probe. The electron gun, identical to the one described previously, consists of a filament (1), a control electrode (2), and a grounded anode (3) with an opening of 6 mm. The gun is normally operated defocused and the beam size is determined by the exit opening of the drift tube (4) which has a

cross section of approximately 1 cm^2. The drift tube is operated at + 90 volts in order to prevent the emission of secondaries. A 95% open grid G0 (5) is placed before the dynode (6) and is operated at - 300 V, preventing the escape of secondaries from the back of the dynode. The G0 and dynode assembly is mounted on a pantograph (7) which can be manipulated from outside the tube with a micrometer, allowing accurate setting of the dynode-to-collector spacing, d. Not shown in the drawing is a mechanism which permits raising the dynode from its centered position by up to 2 cm, keeping d constant. The dynode and its holder can be removed and replaced by lifting it up and out of the tube with a threaded rod through a flange not shown. The collector (8) is an aluminum plate 3 mm thick with a hole in its center slightly larger than 1 mm^2 to accommodate the vibrating tip (16) which has an area just under 1 mm^2. The permanent magnet and pole pieces (9) with their housing came originally from a J. B. Lansing Model LE-30 Hi-Fi speaker. The parts were disassembled, stripped of paints, and cleaned for high vacuum before reassembling and remagnetizing the Alnico V permanent magnet. The air gap was opened to .38 mm, with a measured magnetic field of near 16,000 gauss. The voice coil (10) was drawn from .125 mm hard-drawn aluminum sheet and spot-welded to a six-legged "spider" (11) cut and shaped from the same material by means of a rubber sheet pressing against a steel dye. The coil-winding consists of 20 turns of .125 mm Al wire, with a ceramic "Duroc" coating. A very light coating of "Sauereisen" ceramic coating was used to hold the winding together. The coil wires were taken directly to a feed-through, keeping the voice coil well insulated from ground on both sides. An aluminum bar with 1.5 mm^2 cross section (12) spot-welded to the voice coil is the support for a quartz rod (13) of approximately .5 mm diameter with a second three-legged spider (14)

glued to the rod with a drop of "Sauereisen" cement. The pole tip (16) is partly hollow in order to fit it to the quartz rod (glued with the same cement) and in conjunction with the machining of the collector plate forms a labyrinth to prevent electrons from penetrating the probe assembly. The aluminum shield (15) has been designed in such a way that any penetrating electrons cannot easily reach the insulator rod or the post for support of the electrical connection. If some charging still occurs, the shield also prevents the small piece of thin Al wire, which connects the probe tip to a rigid stainless steel rigid wire, from "seeing" the charged insulator to any significant extent. This wire, with its own vibrational modes, is made to see only aluminum from practically all directions. A 6.5 mm thick, nickel-plated, soft iron shell (17) forms a shield against leakage of static magnetic fields and a 3.2 mm thick, silver-plated copper shell (18) provides electrical shielding between the voice coil and the probe tip. The 6.5 mm thick base plate (19) is the common ground point for the assembly which is transmitted to the outside at the flange (20) through a copper tubing shielding the probe tip connection. Insulators (21) support the structure to the outer stainless steel shell. Vacuum connections are made to a "Vac Sorb" pump for roughing and to a water-cooled 11ℓ/sec ion pump as a final stage. After the first baking for 48 hours at 125°C, a final pressure of approximately 2×10^{-8} torr is obtained. Baking to higher temperature results in damage to the voice coil and to some reduction in the magnetic field at the gap. With the system vented to dry N_2, the ultimate pressure is attained in about 8 hours without further baking. The ion pump is about one foot away from the tube and is enclosed in magnetic shielding.

The circuit for measuring the I versus V characteristics of the dynode and the cpd is shown in Fig. 12. A function generator with the low side connected to a variable low-voltage supply provides a triangular waveform

centered at the desired voltage V_0. The lowest sweep frequency is .01 cps. Dynode current is measured by a floating electrometer with risetimes of the order of 10 msec in the range used. The I versus V characteristic is plotted by a two-pen recorder, also with floating amplifier inputs.

In carrying out a retarding potential measurement, the electrometer will register a step of current due to the differentiation of the ramp by the dynode-to-collector capacitance. In order to remove this step, a second signal is obtained from the ramp generator which supplies this capacitive current directly to the dynode through a 50 pfd capacitor.

The internally generated reference signal of a P.A.R. Lock-In Amplifier, Model HR-8, is used to drive a power amplifier. The shielded output leads are taken to the voice coil feed-through in the tube. One of the leads is grounded at the amplifier side, but the effect on stray signal pickup through ground loops is negligible. The probe signal is picked up by a FET preamplifier and taken to the input of the P.A.R. preamplifier. The recorder output is taken to the second vertical channel of the two-pen recorder or to a storage oscilloscope.

This tube is not intended to produce an accurate measurement of secondary emission coefficient δ. The lack of a grid between the dynode and the collector prevents a good measurement of η_t and the planar geometry insures substantial errors in δ_t due to backscattering. Therefore, only approximate calibration of the primary current I_p is necessary. This has been carried out by placing a solid Al plate at the dynode position and measuring both the dynode current, I_D, and the drift tube current, I_{DT}. Assuming that about 15% of primary electrons are backscattered and no other currents play any significant role, a table of I_{DT} versus E_p for a constant $I_p = 10$ nA was formed. These currents

I_{DT} range between - 2.33 nA at E_p = 4 keV, and - 1.23 nA at 12 keV. Linearity of I_p versus I_{DT} at fixed E_p holds to ± 5% within 3 decades.

The Kelvin probe has been tested extensively in order to determine conditions for the best sensitivity, stability, etc. Since fast response of the probe is not of utmost concern for the measurements to be reported here, operation at approximately 500 cps with a very good sensitivity has been adopted. With a drive of less than .1 watt into the voice coil and d ≃ 1 mm, potential changes of .05 volts can be detected quite unequivocally with a 12 db/octave filter time constant of .1 sec. By careful adjustment of the phase between the reference signal driving the probe and the signal driving the phase sensitive detector at the P.A.R. instrument, it was possible to render the probe quite insensitive to the presence of secondary and transmitted electrons at least up to currents of 100 nA. Since even at a true zero pd between a dynode and the Al collector some stray signal is still picked up by the probe tip, the actual measurements are carried out in a way which is independent of the actual zero offset at the time of measurement, as long as the offset stays constant. With the collector-to-dynode distance d at a given setting, V_D is swept about zero. The dc output of the P.A.R. instrument, V_S, is then plotted versus V_D. Next the spacing d is changed and a second sweep is made. There is a particular value of V_D such that the two traces intersect. At that point the Kelvin probe finds a true zero pd, i.e., its output is independent of spacing, d. If the crossing occurs at $V_D = V_{D0}$, then the dynode surface has a potential $- V_{D0}$ with respect to the collector metal.

The calculation of the energy distribution of emitted electrons with a planar geometry has been reported by Schultz and Pomerantz.[25] Designating N(V) as the total number of secondaries emitted by the dynode but not reaching

the collector because of the retarding field, the energy distribution G(V) is given by

$$G(V) = -V\left(\frac{d^2N}{dV^2}\right) \tag{16}$$

for a cosine distribution of emitted electrons. If the distribution is isotropic, the result is

$$G(V) = -\frac{dN}{dV} - 2V\left(\frac{d^2N}{dV^2}\right) \quad . \tag{17}$$

In this experiment the collector is operated at ground potential while the retarding potential is applied to the same wire from which the dynode current is measured. A typical I versus V characteristic for a high gain dynode is shown in Fig. 13. V_D is the dynode voltage, and for this particular illustration we assume that the cpd is zero and the film is totally uncharged. For V_D very negative, the dynode current I_D is positive, indicating a net loss of electrons. With a primary beam of unity current, a current $(1-\eta_t)$ remains in the dynode, and a current $(\eta_t + \delta_D = \delta_t)$ leaves the dynode. The backscattering from the collector is neglected for the present.

As V_D approaches zero from the negative side, secondaries from the collector due to the fraction η_t of transmitted primaries are more and more able to reach the dynode. At $V_D = 0$, all secondaries from both sources reach their destinations. As V_D is made positive, dynode electrons are being retarded until saturation. Therefore, the dynode yield δ_D, including errors due to backscattering, is

$$\delta_D = \frac{I_D(V_D = 0) - I_D(V_D > +20)}{I_p} \tag{18}$$

Similarly, the effective yield of the collector for transmitted primaries, δ_C, is

$$\delta_C = \frac{I_D(V_D = -20) - I_D(V_D = 0)}{\eta_t I_p} \tag{19}$$

If the angular distribution of secondaries were known to be exactly cosine, one could obtain the product I (d^2I/dV^2) from the $V_D > 0$ part of the I versus V characteristic and determine the energy distribution. For metals in reflection, it is well known that the secondaries have a nearly cosine angular distribution,[5] but no data are available for alkali halides. Even in the absence of a significant surface barrier in the alkali halides, one can justify theoretically a roughly cosine distribtuion of emitted electrons if the internal distribution is isotropic. For electrons of a given energy $\mathcal{E}$ generated at depth d and at an angle $\theta < 90^o$, the path length for mostly forward scattering is proportional to $d/\cos\theta$, and the probability of escape is roughly inversely proportional to the path length.

In order to determine the error involved in assuming an exact cosine distribution in the analysis of results, a computer program was written for obtaining the energy distribution from data like those of Fig. 13 and an arbitrary angular distribution. The program is based on the work of Schultz and Pomerantz[25] who show that the total number of secondaries emitted by the dynode, but not reaching the collector, is

$$N(V) = \int_0^V G(T)\, dT + \int_V^\infty R\, G(T)\, dT \tag{20}$$

where G is the energy distribution of secondaries, and R = 1 - S is the fraction of electrons not reaching the collector. S is given as

$$S = \int_0^{\theta_c} f(\theta) \sin\theta\, d\theta \Big/ \int_0^{\pi/2} f(\theta) \sin\theta\, d\theta \tag{21}$$

where θ_c is the maximum angle of emission for which an electron with kinetic energy T will be collected when the retarding potential is V, given by

$$\theta_c = \cos^{-1} (V/T)^{1/2}, \quad V \leq T \quad . \tag{22}$$

The solution for G(T) given an experimental N(V) and an arbitrary angular distribtuion $f(\theta)$ can now be obtained by the following numerical method:

Divide the range of energies and retarding potentials into steps T_1, T_2, T_3, ..., ; V_1, V_2, V_3, ... Then calculate the values of $S(V_i, T_j)$ by carrying out the integrations of Eq. (24) with the limit $\theta_c(i/j)$ given by Eq. (25). From the values of S, form $R(V_i, T_j)$ and rewrite Eq. (23) in a matrix form by changing the integrals into summations as shown below. Let $N(V_i) = N_i$, $G(T_j) = G_j$, and $R(V_i, T_j) = R_{ij}$. Then

$$\begin{pmatrix} 1 & R_{12} & R_{13} & R_{14} \cdots \\ 1 & 1 & R_{23} & R_{24} \cdots \\ 1 & 1 & 1 & R_{34} \cdots \\ 1 & 1 & 1 & 1 \cdots \\ \vdots & \vdots & \vdots & \vdots \\ 1 & 1 & 1 & 1 \cdots \end{pmatrix} \begin{pmatrix} G_1 \\ G_2 \\ G_3 \\ G_4 \\ \vdots \\ 1 \end{pmatrix} = \begin{pmatrix} N_1 \\ N_2 \\ N_3 \\ N_4 \\ \vdots \\ 1 \end{pmatrix} \tag{23}$$

This forms a system of linear equations which can be solved for G. In practice, a range of 10 volts is taken in .1-volt steps for both T and V and the solution is obtained by a method of least squares.

Results of the computations obtained from data similar to those of Fig. 13, for a cosine distribution and deviations from it show that the solution is not

very sensitive to the actual shape of the angular distribution except in the case of extreme deviations from the cosine function at θ near 90 degrees, as for example, with distributions equal to 0 or 1 between 80 and 90 degrees. Therefore, a cosine distribtuion has been assumed in order to obtain the secondary energy distribtuion from the experimental results by means of the computer program discussed. Alternatively, one could differentiate the curves electronically one time and smooth out the data before a second differentiation by computer. This has been tried, but is about as "noisy" as the process indicated above, and requires more steps.

Measurements on newly deposited films of CsI and KCl show that the potential with respect to the collector of the film surface ranges between + .1V and - .1V; essentially the same as the contact potential of the substrate with no halide film. Although CsI and KCl layers do not affect the work function of the Al backing when the films are new, this is not the case for NaF. Here V_{D0} is approximately -.5 volts, which may be attributed to dissociation of some NaF during evaporation, with the result that Na atoms lower the work function of the Al backing.

Under prolongued bombardment, CsI films show two different kinds of changes: (1) an irreversible change of V_{D0} (becoming more negative) which does not affect the I versus V_D characteristic of the film, except for a shift in position, and (2) a reversible change of V_{D0} in the same direction whose effect on the I versus V_D characteristics is indicative of patch positive charging of the dynode surface. This patch effect does not result in enhancement of secondary yield, however. The irreversible change, of up to about 1 V, is again linked to dissociation of the alkali halide, with a concomitant chemical reaction on the Al layer. The outline of the electron beam, including the shadow of a grid, is clearly visible on the substrate after exposure of the film to room air, even after the alkali halide film has been washed off with water.

For the results reported here, charging of the film has been investigated only to define a method for avoiding such effects. The following technique proved suitable:

(1) After evaporation, the film is directly transferred to the Kelvin Probe tube under dry nitrogen with less than 1.5% relative hunidity.

(2) After pump down to approximately 2×10^{-8} torr the first pd measurement is carried out by the standard method described above.

(3) At a primary current density of about 1 nA/cm^2 a retarding potential measurement for a desired E_p is carried out by linearly sweeping V_D from -1 to + 9 volts, and back, in 10 seconds maximum. Only during that time is the beam on.

(4) A new pd measurement is made to check that no substantial charging has occured, and the procedure is repeated for other E_p's.

The effects of electrons backscattered to the dynode from the collector have been found to be negligible by comparing energy distributions obtained with the normal, low backscattering, Al collector, and with a collector coated with gold (high backscattering).

For each of the four materials studied, three consecutive measurements were made; E_p = 4 or 5 keV (point of low yield), E_p = 7 or 8 keV (highest yield), and E_p = 12 keV (maximum primary penetration). The film thickness selected was 500 Å, to insure isolation of effects due to the substrate. Potential differences changed during the measurements by less than 0.05 volts, a negligible amount.

The results analyzed by the method indicated above assuming a cos θ angular distribution of emitted electrons, are shown in Fig. 14 to 17. The results are normalized to unity area.

Within fluctuation and analysis errors the energy distributions are independent of E_p, for a given film. The marked dependence on Z is qualitatively explained by noting that the escape probability for low energy electrons decreases rapidly with decreasing Z on the basis of the electron-phonon interaction calculations of Part 1.

The energy distribution approaches zero near $\mathcal{E} = 6.5$ eV for CsI, $\mathcal{E} =$ 7.5 eV in KCl, $\mathcal{E} = 8.5$ eV in NaF, and above $\mathcal{E} = 9$ eV for LiF. The location of the first excitonic absorption edge for these materials is approximately 5.7, 7.6, 10.5 and 11 eV, respectively, and agrees roughly with the energy distribtuion of the emitted secondaries. Better agreement is not expected because of the inherent inaccuracies of the planar analysis above 5 volts, or so.

The appearance of a dip near $\mathcal{E} \simeq 3.5$ eV in KCl (Fig. 15) is not an error. The experimental I versus V_D curves nearly have an inflection point at that energy. This will be discussed further.

VI. COMPUTATIONS OF YIELDS AND DISCUSSION OF RESULTS

The following procedure was followed for each of the materials studied: Calculation of $G(\mathcal{E}_{0j})$ is made in accordance with Eq. (9) from the experimentally determined value of δ for the film thickness nearest 500 Å, at E_p near 8 keV. To perform this calculation the values of attenuation length, $L_s(\mathcal{E}_{0j})$, are initially obtained from Table 1 of Part I. With these values of G and L_s, curves of δ versus E_p for all other thicknesses and primary energies are completely determined. By simultaneously varying all L_s over the range ± 30% in several steps, new values of $G(\mathcal{E}_{0j})$ are computed. This simultaneous variations corresponds to varying the effective mass as discussed in section VI, Part I.

The value of effective mass giving the best fit to the ensemble of experimental curves is obtained, and appears as the dashed line in Figs. 6 through 9. The entire ensemble of theoretical curves for each material is thus given from normalizing to the yield at one energy and one thickness, and then optimizing by variation of one free parameter only.

The best computed results are obtained with an effective mass $m^*/m = 1$ for CsI, and 1.2 for KCl, NaF, and LiF. In Fig. 6, for CsI, two points are also plotted corresponding to the yield obtained by using L_s values for KCl with the excitation function for CsI and following the procedure outlined above. This gives an indication of the sensitivity of the present calculations to the values of L_s used.

In the process of fitting, changes in L_s of up to $\pm$ 30% do not affect the shapes of the individual curves but do change the relative magnitudes of the curves in a set (except for the "pivotal" $\tau = 500$ Å curve, which remains unchanged). Discrepancies between the shapes of experimental and theoretical curves are therefore due to errors in the calculation of $-(dE/dx)$ by the procedure described in section II. The determination of $-(dE/dx)$ for KCl, NaF, and LiF is substantially less accurate than for CsI, due to their lower densities and atomic numbers.

The computed yields for CsI, Fig. 6, show good agreement with the experimental results in all the essential features. This supports the simple picture of secondary emission controlled only by the energy loss suffered by the primary electrons and by the interaction between the nearly free excited electrons ($m^* \simeq m$) and the longitudinal optical modes of the phonon field.

A similar conclusion can be reached in the cases of NaF and LiF. Application of the characteristic escape lengths L_s of Part I, modified to $m^*/m = 1.2$, correctly fits the experimentally determined saturation of yield with increasing

film thickness at E_p = 10 to 12 keV. For these primary energies - (dE/dx) is constant for fixed E_p, and practically independent of thickness.

The experimentally determined energy distribution of emitted secondaries from KCl (Fig. 15) indicates that the simple picture given above may not be fully adequate for that material. A dip in the distribution near 3.5 eV is clearly observable and could be attributed to the existence of flat energy bands near that energy, resulting in electrons of large effective mass.

Band calculations for KCl by Oyama and Miyakawa[26] show that the region between 2 and 5 eV above the bottom of the conduction band is occupied by d-like bands (Γ_{25}' , Γ_{12}) and in particular, very flat portions of the Γ_{12} bands appear in the region near 3.5 eV. Onodera and Toyozawa[27] discuss the possibility that such low lying d-like bands exist in K, Rb and Cs halides, but not in Li and Na halides. It is possible that strong excitonic absorption exists, but no theoretical treatment of excitons near 3.5 eV is found in the literature.

The calculations of yield for KCl shown in Fig. 7 have been carried out by using the same procedure as in the other three materials, using m^*/m = 1.2, and the experimental distribution of Fig. 15. The results show the same type of agreement with experiments as NaF and LiF.

The internal excitation functions $G(\mathcal{E}_{0j})$, shown in Fig. 18, are monotonically decreasing functions of energy with the exception of the curve for KCl. If the escape lengths for electrons with initial energies near 3.5 eV are artificially reduced to simulate the effect of d-like bands until a monotonic excitation function is obtained, the computed yields change very little.

It is interesting to obtain a composite escape probability for all the electrons generated at a location x by rearranging the summations in Eq. (8)

$$\delta = \sum_{x_i} \left(-\frac{dE}{dx}(x_i)\right) \left\{ \sum_{\mathcal{E}_{0j}} G(\mathcal{E}_{0j})\, P_0(\mathcal{E}_{0j}) \exp\left[-\frac{\tau - x_i}{L_s(\mathcal{E}_{0j})}\right] \Delta\mathcal{E}_{0j} \right\} \Delta x \qquad (24)$$

The expression in brackets is the composite escape probability P(x), which has usually been assumed to be a simple exponential. Here, it is a weighted sum of exponentials. The functions P(x) for 1000 Å films of the four materials studied are shown in Fig. 19. Some local values of L_s have been shown in the graph. The decrease in local L_s as one moves towards the exit of the film is due to the increased participation of lower energy secondaries to the secondary yield.

With regard to the average energy needed to generate one secondary electron, it must be pointed out that the methods used do not allow a determination of the lowest energy part of the internal excitation function, because electrons with very low initial energy do not come out from the film. Also, the results for $G(\mathcal{E}_{0j})$ at the low energy end are not very reliable, because the computed values of δ are not very sensitive to the values of L_s for the lowest energy electrons, while the results of $G(\mathcal{E}_{0j})$ are very sensitive. Thus, an uncertainty remains regarding the actual behavior of electrons with very low initial energy.

The integral $\int G(\mathcal{E}_0)d\mathcal{E}_0$ over <u>all</u> the energies between 0 and the energy of the first absorption peak (approximately) would give the number of internal secondary electrons generated per keV of energy lost by the primary beam. In the absence of sufficient information at the low energy end, carrying out the integral over the parts of the curves shown in Fig. 18 only, the number of internal secondary electrons with energies such that they will contribute to secondary emission per unit of primary energy lost can be obtained. From these numbers, the approximate energy losses to create one internal secondary in CsI, KCl, NaF, and LiF are, respectively, 66, 25, 38, and 36 eV per electron generated, in rough agreement with the calculation by Sternglass[11] of 20 to 35 eV, which includes electrons generated with energies too low to contribute to the yield.

From a transport theory based on a simplified electron-phonon interaction in insulators, by assuming an internal generation function

$$G(\mathcal{E}) = \text{constant for } 0 < \mathcal{E} \leq \mathcal{E}_0 \qquad (25)$$
$$G(\mathcal{E}) = 0 \qquad \text{for } \mathcal{E} > \mathcal{E}_0$$

where $\mathcal{E}_0$ is some fixed energy depending on the material, and by taking $\mathcal{E}_0 = 10$ eV and an electron affinity of 1 eV for the crystal, Dekker[28] finds an external energy distribution peaked broadly at $\mathcal{E} = 5$ eV. For a different assumption for the internal generation function,

$$G(\mathcal{E}) = \text{constant} \cdot (E_0 - E), \qquad (26)$$

the external energy distribution shifts to a broad peak near 4 eV. Dekker concludes that the external energy distribtuion is not very sensitive to the form of the internal generation function.

In the light of the work presented here, Dekker's conclusion appears unjustified. Since the escape depth of electrons generated at the higher energies is so much greater than that of electrons with low initial energy, the use of expressions (25) or (26) for $G(\mathcal{E})$ can be expected to lead to very substantial errors in the external energy distribution and in secondary yield.

VII. CONCLUSION

The work reported here demonstrates that (with the possible exception of materials with low lying d-like bands), the secondary emission coefficient of a given alkali halide is determined by four main factors: Average atomic number, frequency of the longitudinal optical modes, density, and band gap. The average atomic number determines the energy loss of the primary beam per unit depth (in μg/cm). The frequency of the longitudinal optical modes determines $\hbar\omega$,

the energy exchanged per collision and along with ϵ_∞ and ϵ_0, it defines collision rates. In general, the larger ω is, the more energy losses electrons suffer on their way to the surface and the lower is the value of L_s (in Å). For nearly fixed Z and L_s, the higher the material density, the more primary energy loss will occur within the escape depth L_s, resulting in higher yield. For the observed monotonically decreasing internal generation functions extending up to or near the conduction band energy, materials with larger gaps have a contribution to the yield from electrons with substantially higher initial energies $\mathcal{E}_0$ than in the case of smaller gaps. Since lower Z materials have the largest gaps, this effect tends to compensate for the smaller primary energy losses and the shorter values of L_s for a given $\mathcal{E}_0$ in such materials.

The experimental work presented here shows that the detailed quantitative results of perturbation theory developed in Part I are substantially correct. The experiments do not furnish much information regarding the behavior of electrons with very low initial energy, which is precisely the case in which first order electron-phonon theory may not apply. A new class of experiments examining the transport of practically monochromatic electrons in alkali halides is being planned.

ACKNOWLEDGEMENTS

The authors are very grateful to John Edgecumbe for very valuable ideas during the planning of the measurements reported, to A. Roder and C. Thurman for making the substrate films, and to the Technical Staff of the Physical Electronics Group and Research Machine Shop of the Stanford Linear Accelerator Center, for their invaluable assistance.

PART II: REFERENCES

1. L. Austin and H. Starke, Ann. Physik 9, 271 (1902).
2. K. G. McKay, Advances in Electronics 1, 65 (1948).
3. H. Bruining, Physics and Applications of Secondary Electron Emission (McGraw-Hill, New York 1954).
4. R. Kollath, Encyclopedia of Physics 21, (Flugge Ed. Springer, Berlin 1956) p. 232.
5. A. J. Dekker, Solid State Physics 6, (Academic, New York 1958) p. 251.
6. H. Kanter, Phys. Rev. 121, 461 (1961).
7. H. Kanter, Phys. Rev. 121, 677 (1961).
8. H. Kanter, Phys. Rev. 121, 681 (1961).
9. H. Kanter and E. J. Sternglass, Phys. Rev. 126, 620 (1962).
10. H. Jahrreiss, Ann. Physik 7, 325 (1964).
11. E. J. Sternglass, Westinghouse Research Labs., Scientific Paper 6-94410-2-P9 (July 1957).
12. D. E. Anderson, A. B. Laponsky, W. T. Peria, and et al., Physics of Electron Emission, AFAL-TR-66-250-Vol. 1 (University of Minnesota, Minneapolis, Minnesota, 1966).
13. T. R. Young, Phys. Rev. 103, 292 (1956).
14. J. E. Halliday and E. J. Sternglass, J. Appl. Phys. 28, 1189 (1957).
15. M. V. Gomoyunova and N. A. Letunov, Soviet Phys.-Solid State 7, 311 (1965).
16. M. V. Gomoyunova and N. A. Letunov, Soviet Phys.-Solid State 7, 316 (1965)
17. J. Edgecumbe and E. L. Garwin, J. Appl. Phys. 37, 2916 (1966).

18. J. Edgecumbe and E. L. Garwin, J. Appl. Phys. 37, 3321 (1966).

19. H. Jacobs, Phys. Rev. 84, 877 (1951).

20. G. W. Goetze, A. H. Boerio, and M. Green, J. Appl. Phys. 35, 482 (1964).

21. A. Roder, Report No. SLAC-TN-67-26, Stanford Linear Accelerator Center, Stanford University, Stanford, California (1967).

22. J. R. Young, J. Appl. Phys. 28, 512 (1957).

23. K. H. Geyer, Ann. Physik 5, 117 (1942).

24. B. Petzel, Ann Physik 7, 55 (1960).

25. A. A. Schultz and M. A. Pomerantz, Phys. Rev. 130, 2131 (1963).

26. S. Oyama and T. Miyakawa, J. Phys. Soc. Japan 21, 868 (1966).

27. Y. Onodera and Y. Toyazowa, J. Phys. Soc. Japan 22, 833 (1967).

28. A. J. Dekker, Physica 21, 29 (1954).

LIST OF FIGURES

18. Internal excitation function $G(\mathcal{E}_0)$ for the four selected alkali halides.

19. Composite escape function P(x) for the four selected alkali halides.

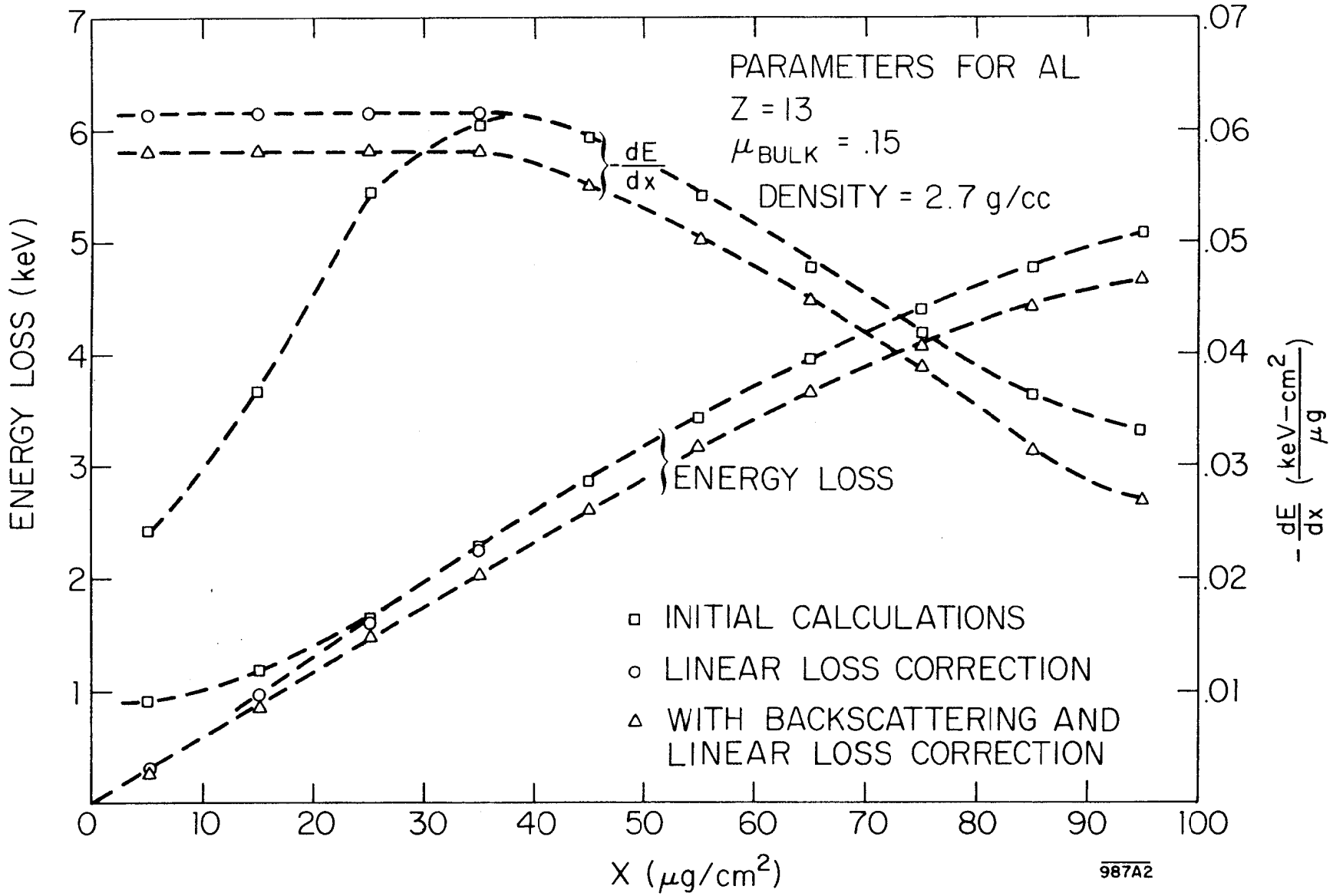
PARAMETERS FOR AL
Z = 13
μ_{BULK} = .15
DENSITY = 2.7 g/cc
$-\frac{dE}{dx}$
ENERGY LOSS
INITIAL CALCULATIONS
LINEAR LOSS CORRECTION
WITH BACKSCATTERING AND LINEAR LOSS CORRECTION
ENERGY LOSS (keV)
$-\frac{dE}{dx}$ ($\frac{keV-cm^2}{\mu g}$)
X ($\mu g/cm^2$)
987A2

Fig. 1

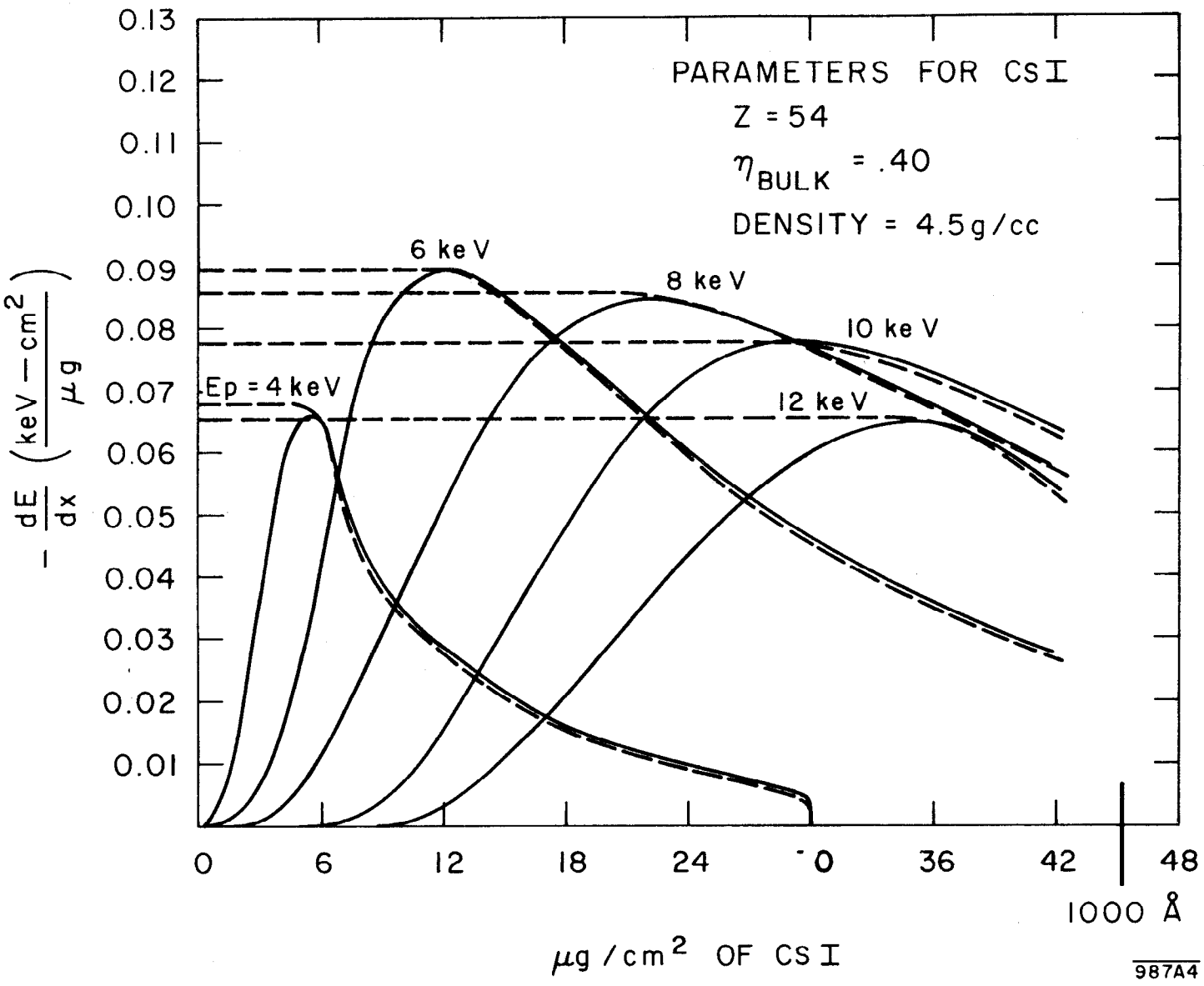
PARAMETERS FOR CSI
Z = 54
η_{BULK} = .40
DENSITY = 4.5g/cc
6 keV
8 keV
10 keV
12 keV
Ep = 4 keV
$-\frac{dE}{dx}\left(\frac{keV-cm^2}{\mu g}\right)$
0.13
0.12
0.11
0.10
0.09
0.08
0.07
0.06
0.05
0.04
0.03
0.02
0.01
0
6
12
18
24
30
36
42
48
1000 Å
$\mu g/cm^2$ OF CSI
987A4

Fig. 2

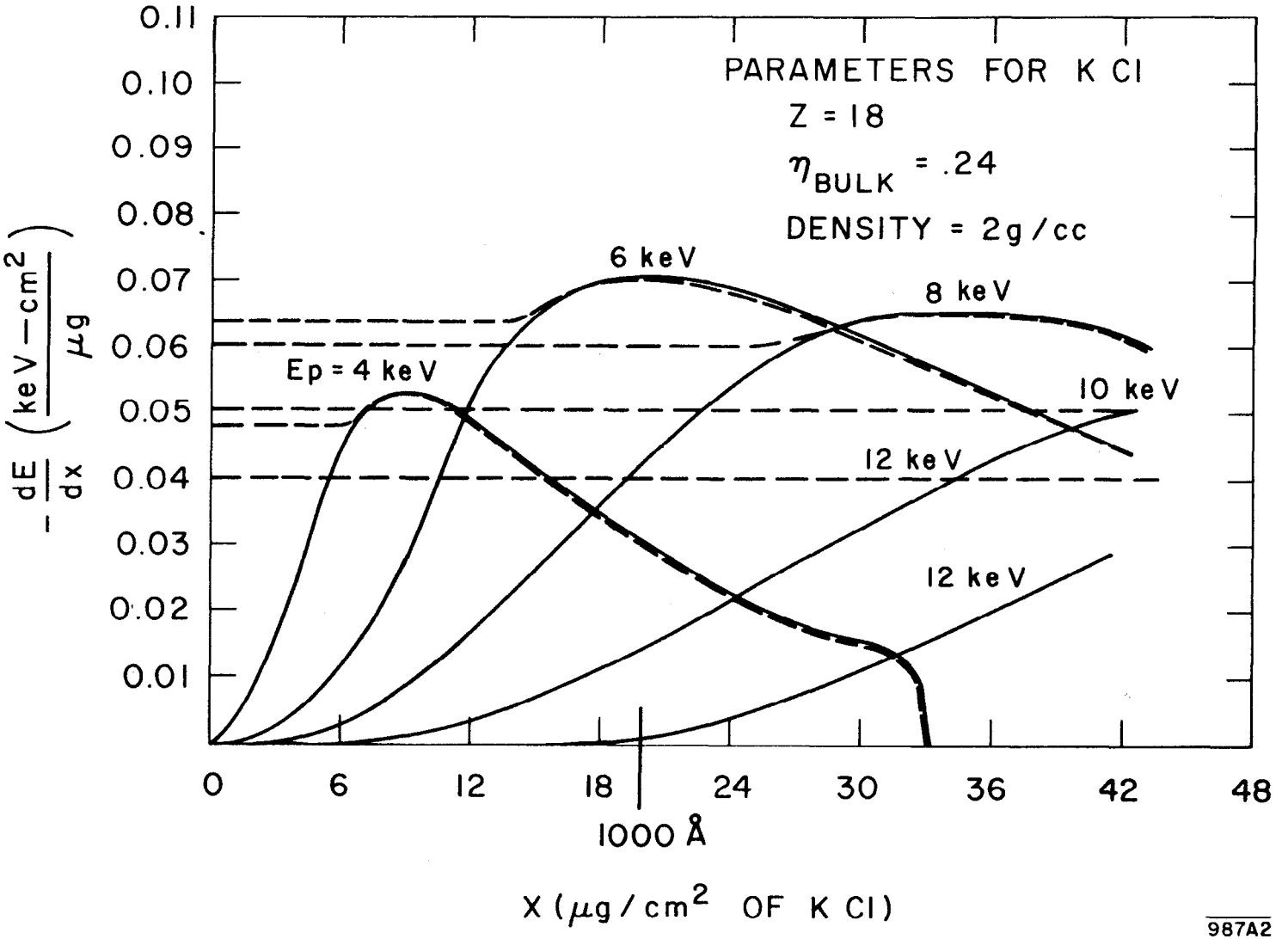
PARAMETERS FOR K Cl
Z = 18
η_{BULK} = .24
DENSITY = 2g/cc
6 keV
8 keV
10 keV
12 keV
12 keV
Ep = 4 keV
$-\frac{dE}{dx}\left(\frac{keV-cm^2}{\mu g}\right)$
0.11
0.10
0.09
0.08
0.07
0.06
0.05
0.04
0.03
0.02
0.01
0
6
12
18
24
30
36
42
48
1000 Å
X ($\mu g/cm^2$ OF K Cl)
987A2

Fig. 3

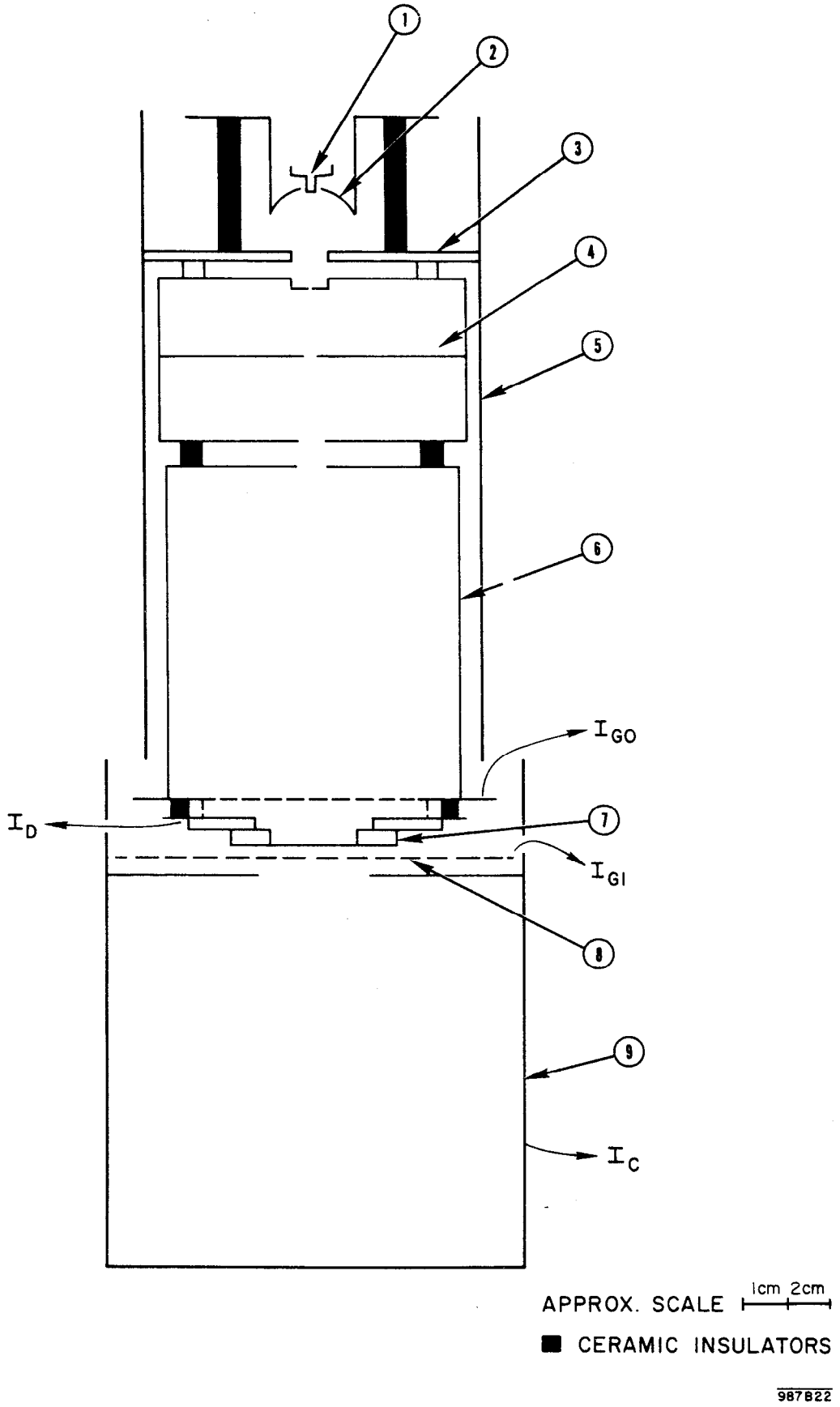
1
2
3
4
5
6
I_{GO}
I_D
7
I_{GI}
8
9
I_C
APPROX. SCALE 1cm 2cm
CERAMIC INSULATORS
987822

Fig. 4

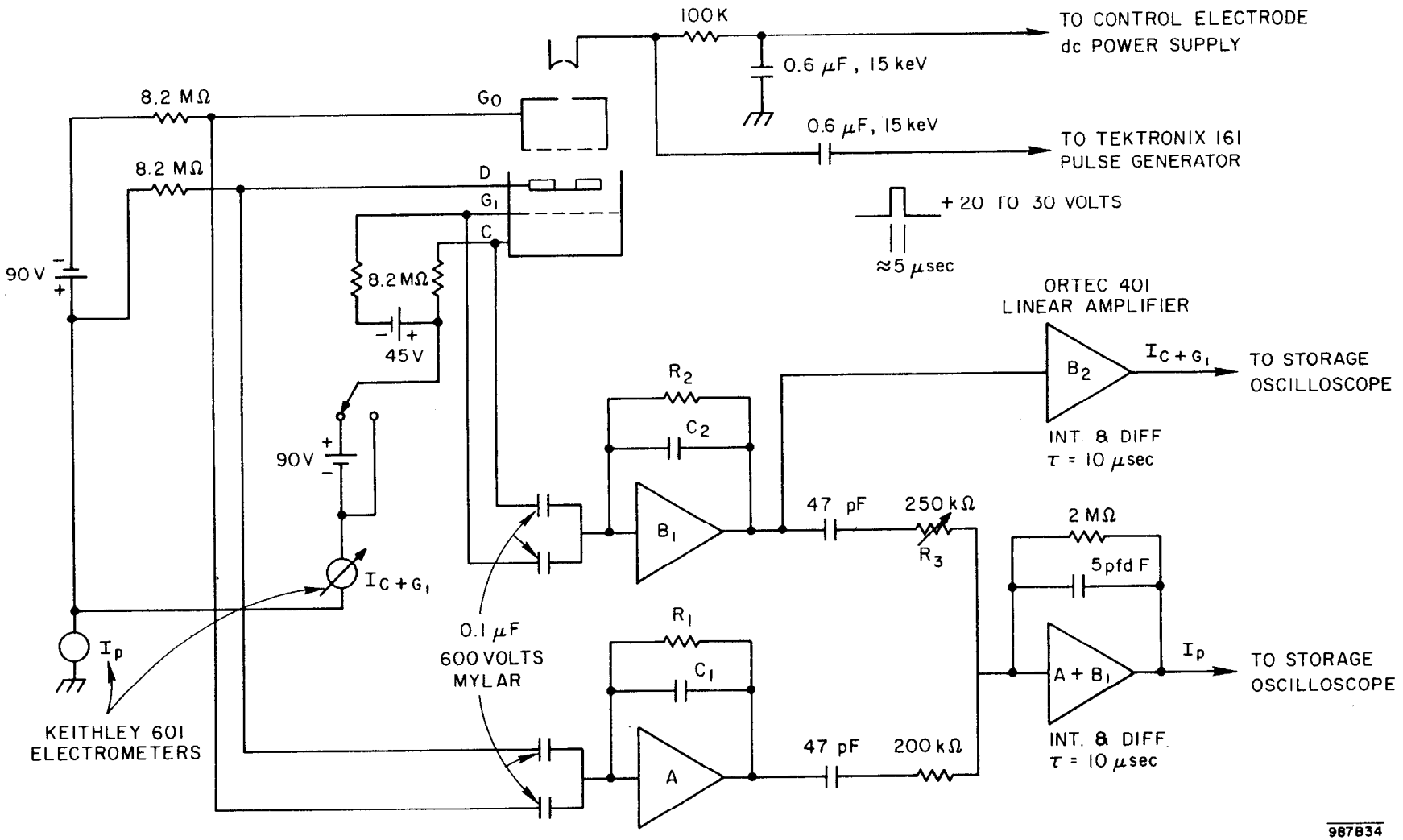

FET CHARGE
SENSITIVE AMPLIFIERS

Fig. 5

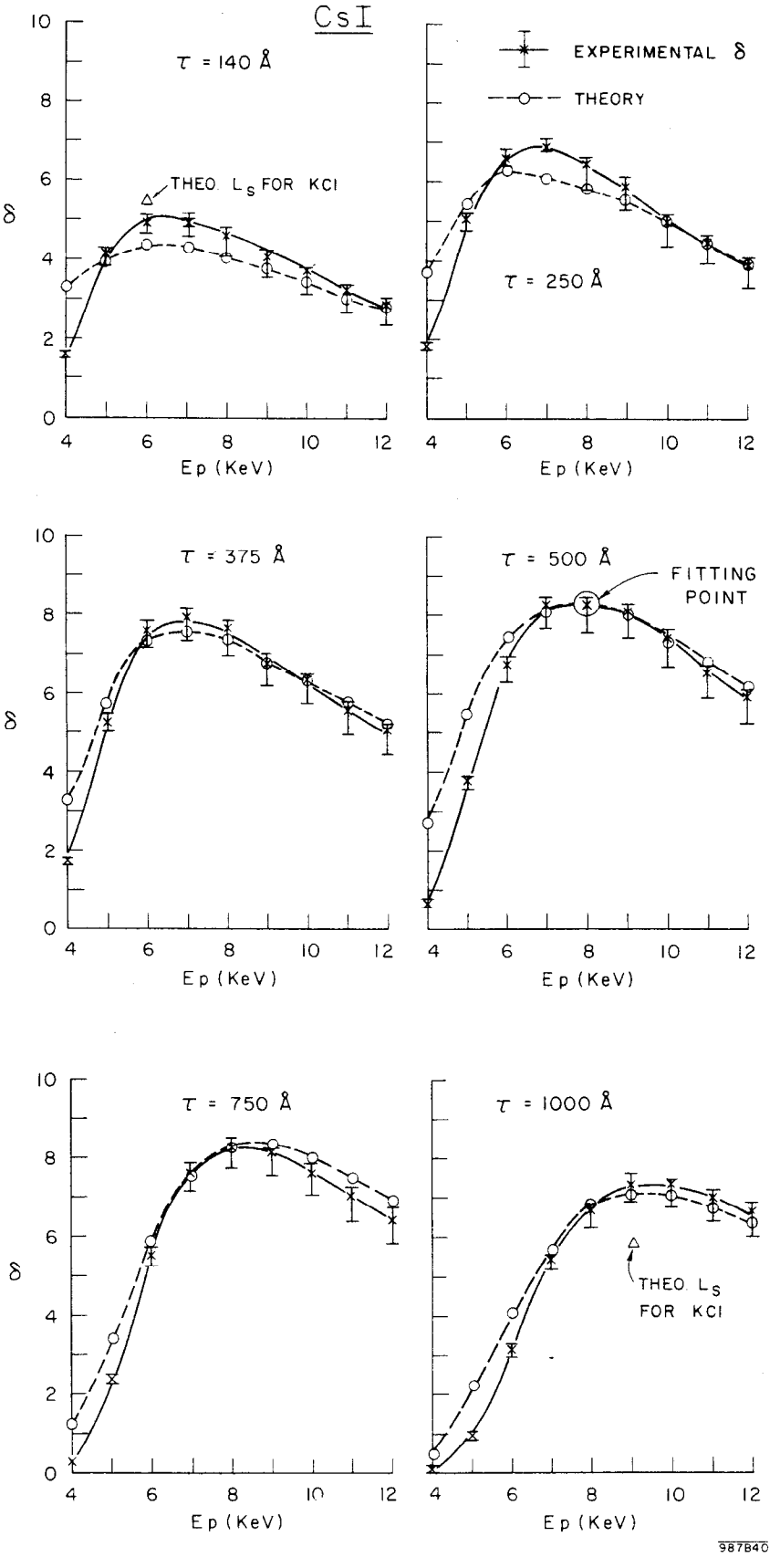
CsI
τ = 140 Å
THEO. L_S FOR KCl
EXPERIMENTAL δ
THEORY
τ = 250 Å
τ = 375 Å
τ = 500 Å
FITTING POINT
τ = 750 Å
τ = 1000 Å
THEO. L_S FOR KCl
δ
Ep (KeV)
0
2
4
6
8
10
12
987B40

Fig. 6

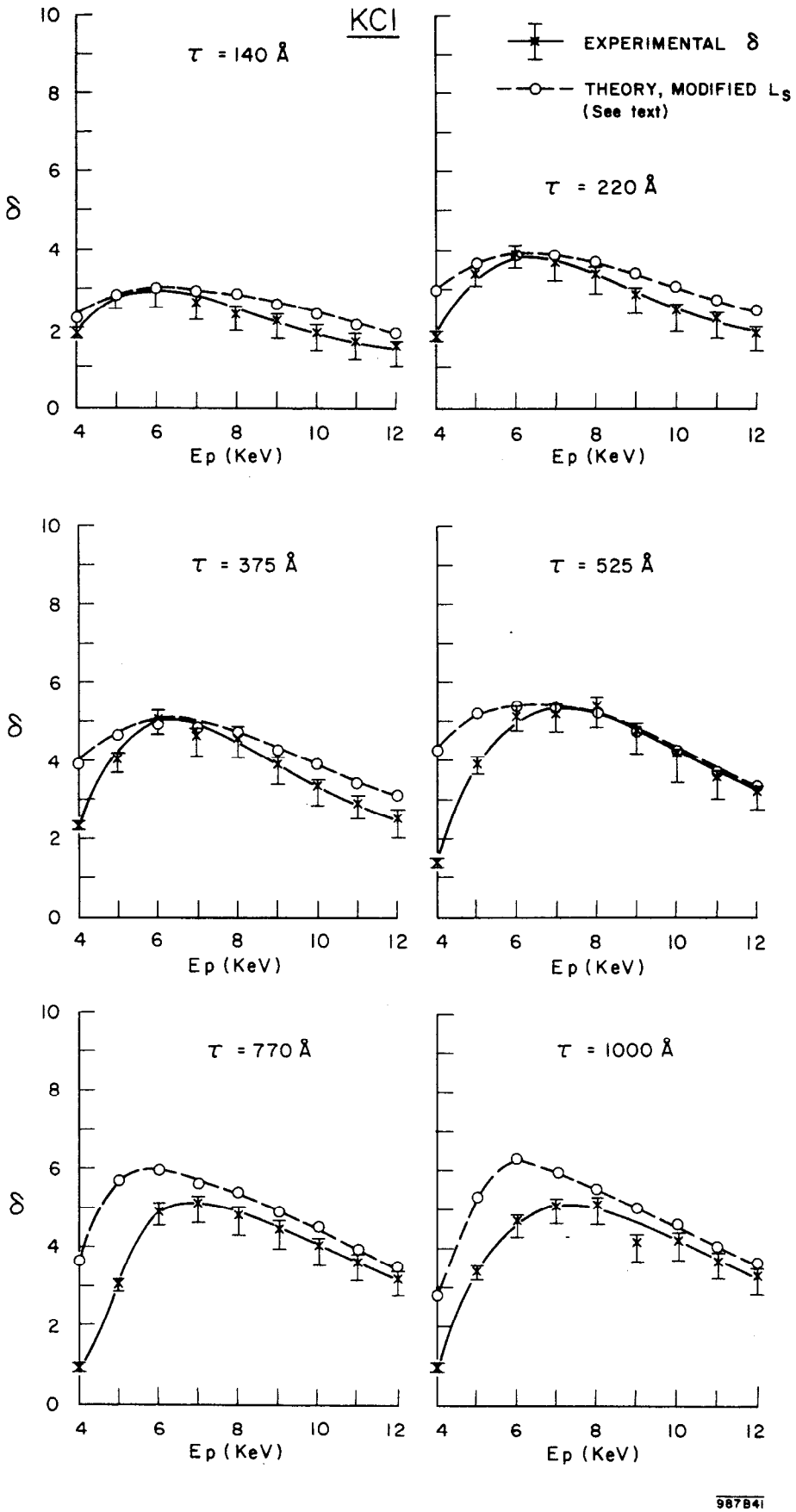
KCl
EXPERIMENTAL δ
THEORY, MODIFIED Ls
(See text)
τ = 140 Å
τ = 220 Å
τ = 375 Å
τ = 525 Å
τ = 770 Å
τ = 1000 Å
δ
Ep (KeV)
0
2
4
6
8
10
12
987B41

Fig. 7

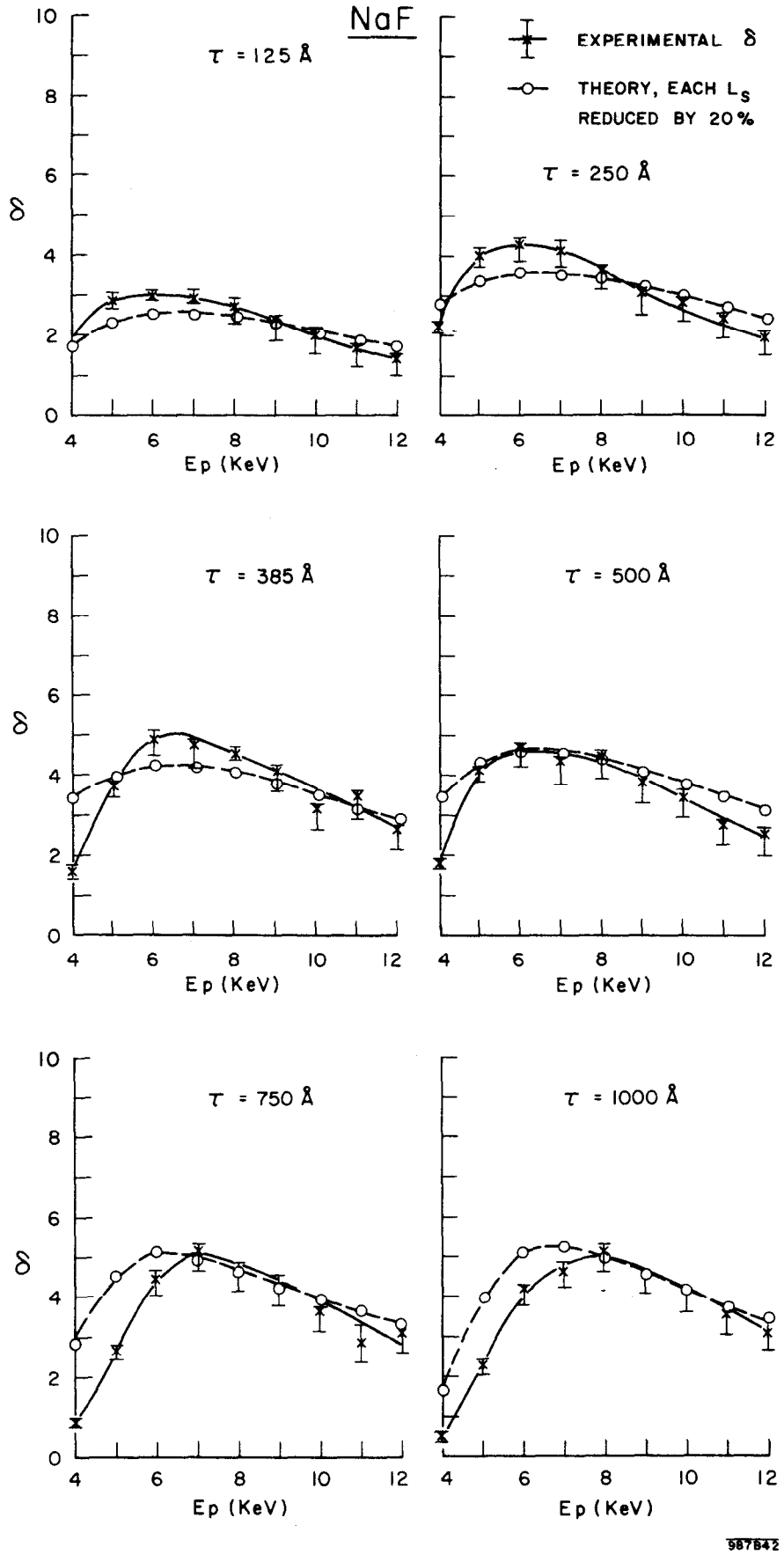
NaF
EXPERIMENTAL δ
THEORY, EACH L_S REDUCED BY 20%
τ = 125 Å
τ = 250 Å
τ = 385 Å
τ = 500 Å
τ = 750 Å
τ = 1000 Å
δ
Ep (KeV)
0
2
4
6
8
10
12
987842

Fig. 8

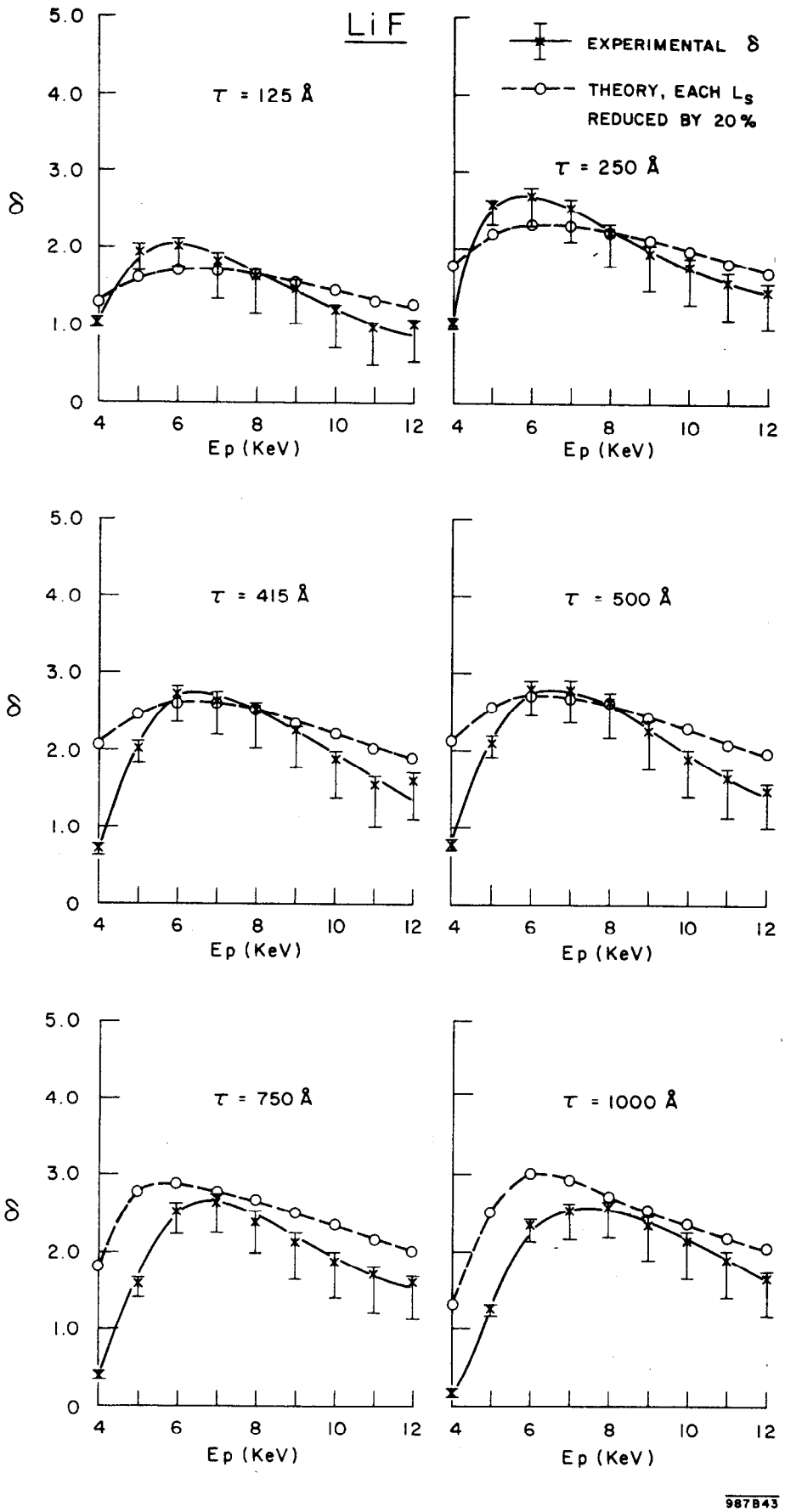
LiF
EXPERIMENTAL δ
THEORY, EACH L_s REDUCED BY 20%
τ = 125 Å
τ = 250 Å
τ = 415 Å
τ = 500 Å
τ = 750 Å
τ = 1000 Å
δ
Ep (KeV)
0
1.0
2.0
3.0
4.0
5.0
4
6
8
10
12
987B43

Fig. 9

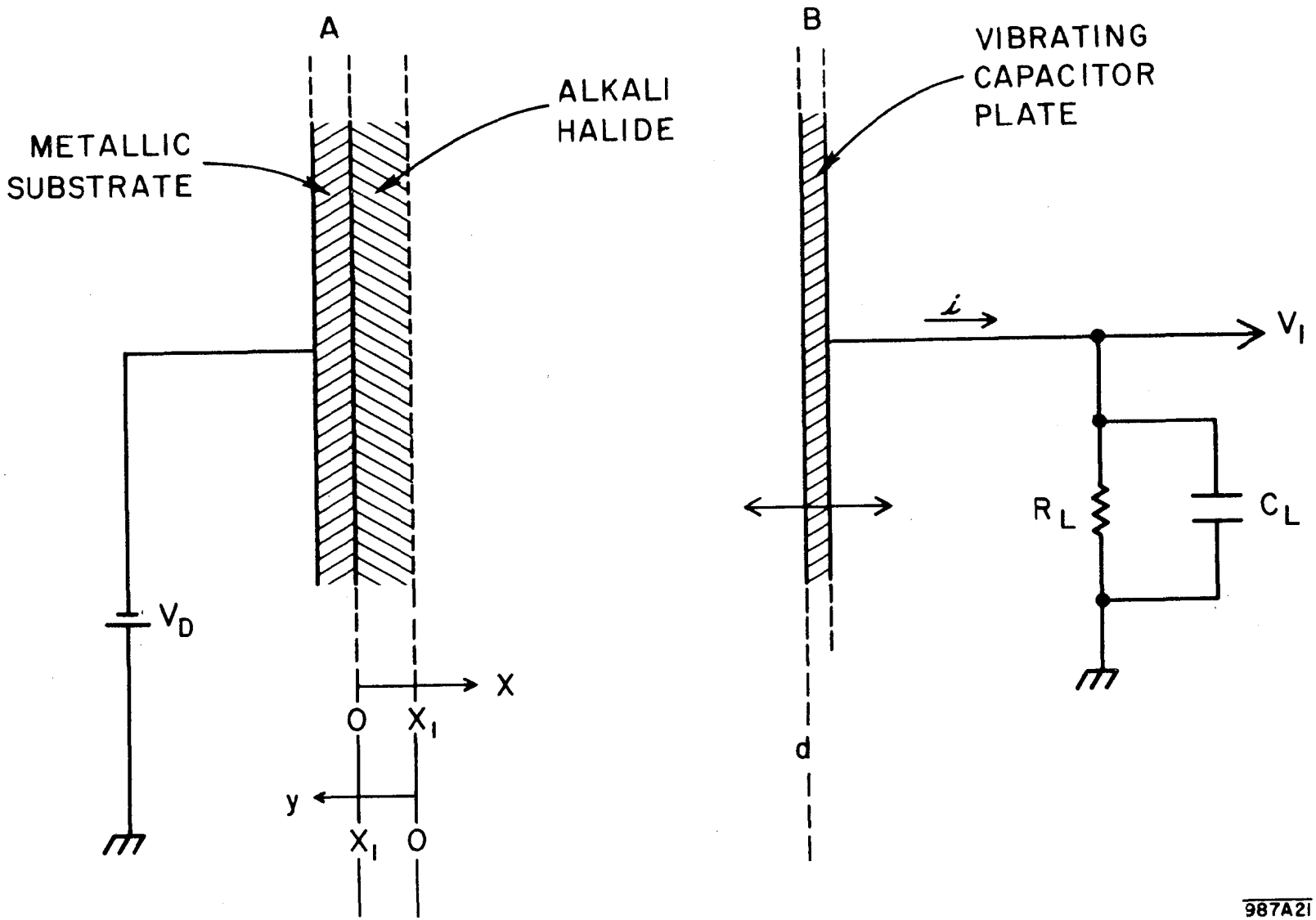
A
METALLIC SUBSTRATE
ALKALI HALIDE
V_D
X
O
X_1
y
X_1
O
B
VIBRATING CAPACITOR PLATE
i
V_I
R_L
C_L
d
987A21

Fig. 10

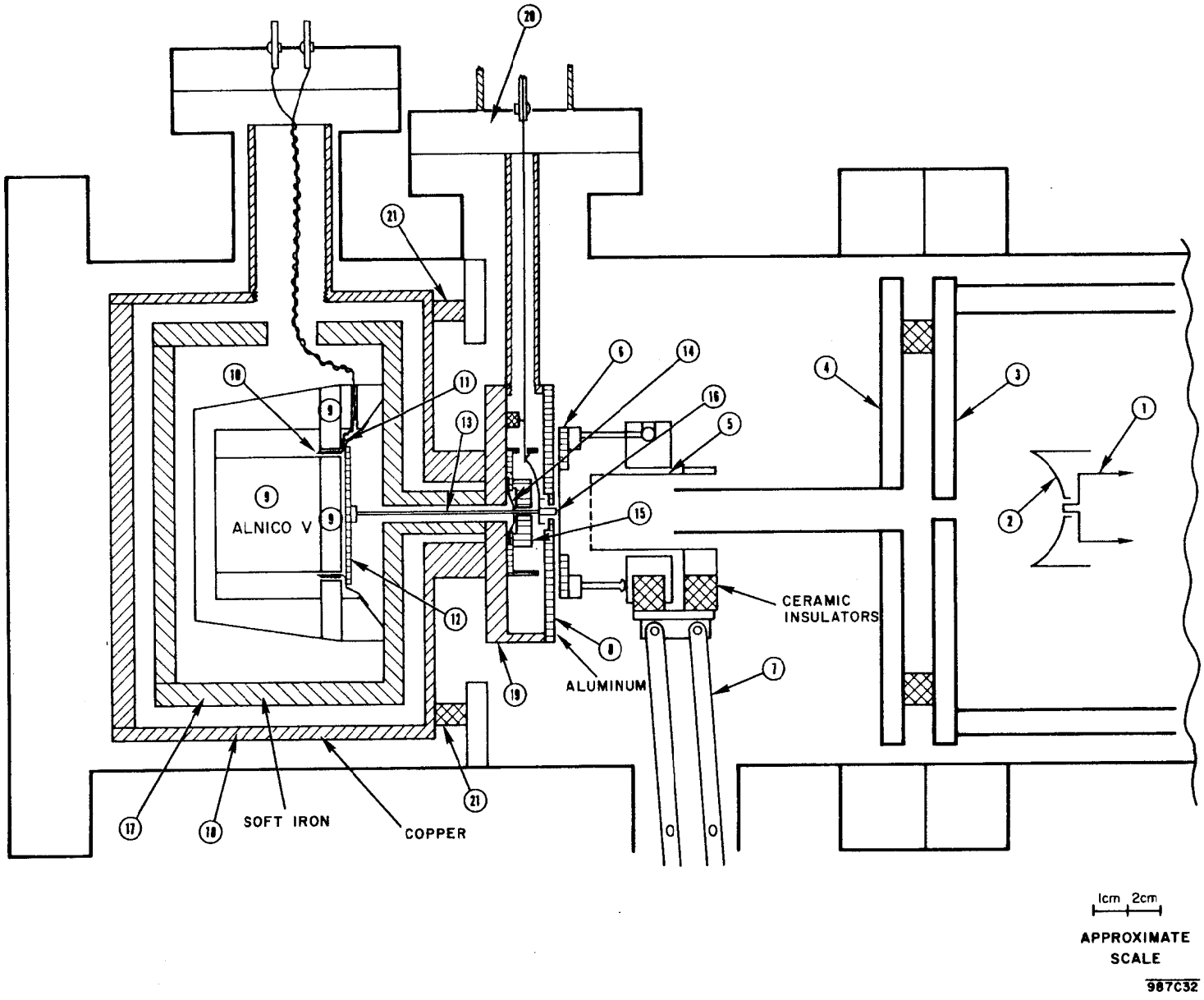
20
21
18
11
9
13
6
14
16
5
4
3
1
2
9
ALNICO V
9
15
12
CERAMIC
INSULATORS
8
ALUMINUM
19
7
17
18
SOFT IRON
COPPER
21
1cm 2cm
APPROXIMATE
SCALE
987C32

Fig. 11

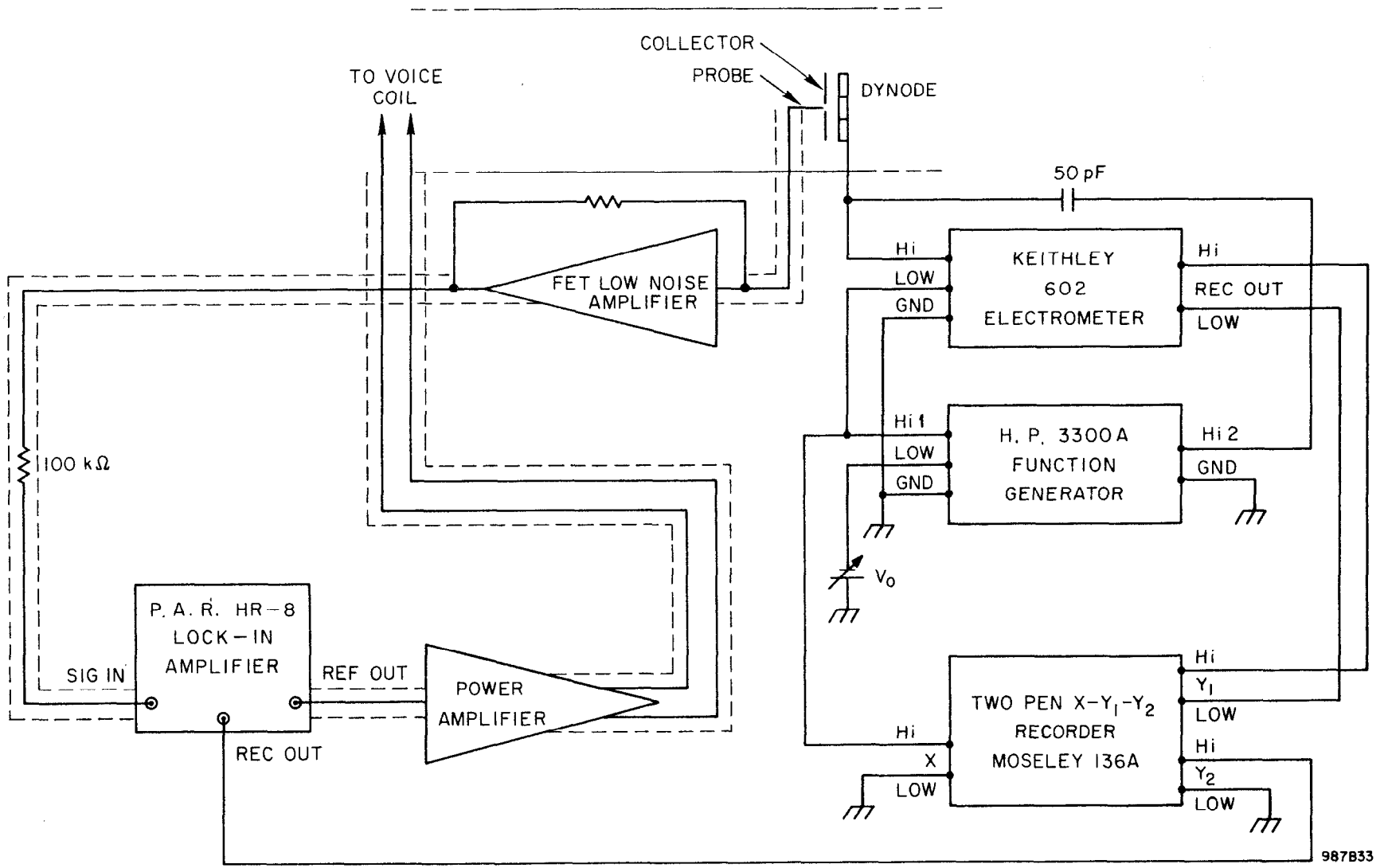
COLLECTOR
PROBE
DYNODE
TO VOICE COIL
50 pF
FET LOW NOISE AMPLIFIER
Hi
LOW
GND
KEITHLEY 602 ELECTROMETER
Hi
REC OUT
LOW
100 kΩ
Hi 1
LOW
GND
H. P. 3300A FUNCTION GENERATOR
Hi 2
GND
V_o
P. A. R. HR-8 LOCK-IN AMPLIFIER
SIG IN
REF OUT
POWER AMPLIFIER
REC OUT
Hi
Y_1
LOW
TWO PEN $X-Y_1-Y_2$ RECORDER MOSELEY 136A
Hi
X
LOW
Hi
Y_2
LOW
987B33

Fig. 12

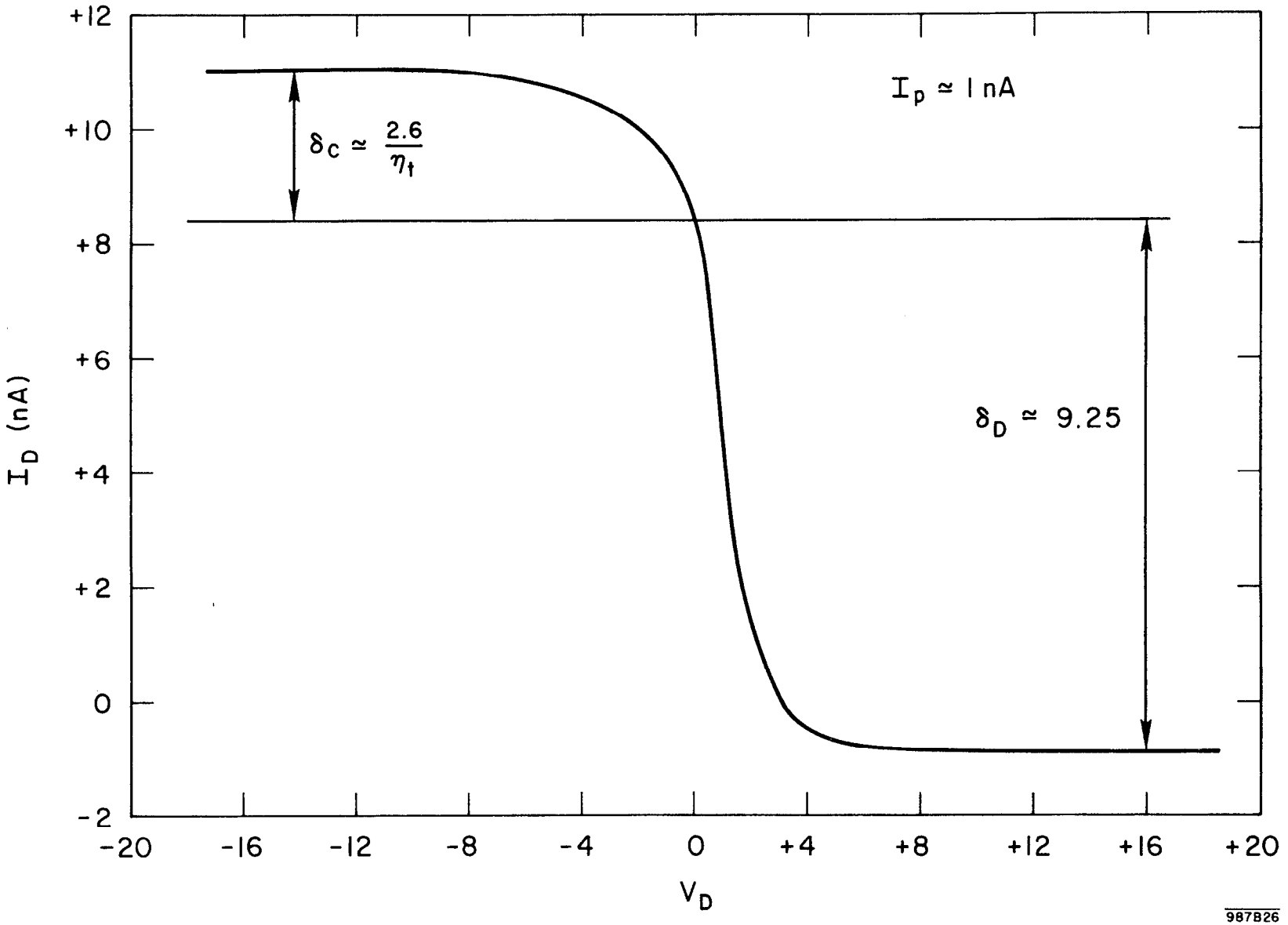
+12
+10
+8
+6
+4
+2
0
-2
I_D (nA)
$I_p \simeq 1$ nA
$\delta_C \simeq \frac{2.6}{\eta_t}$
$\delta_D \simeq 9.25$
-20
-16
-12
-8
-4
0
+4
+8
+12
+16
+20
V_D
987826

Fig. 13

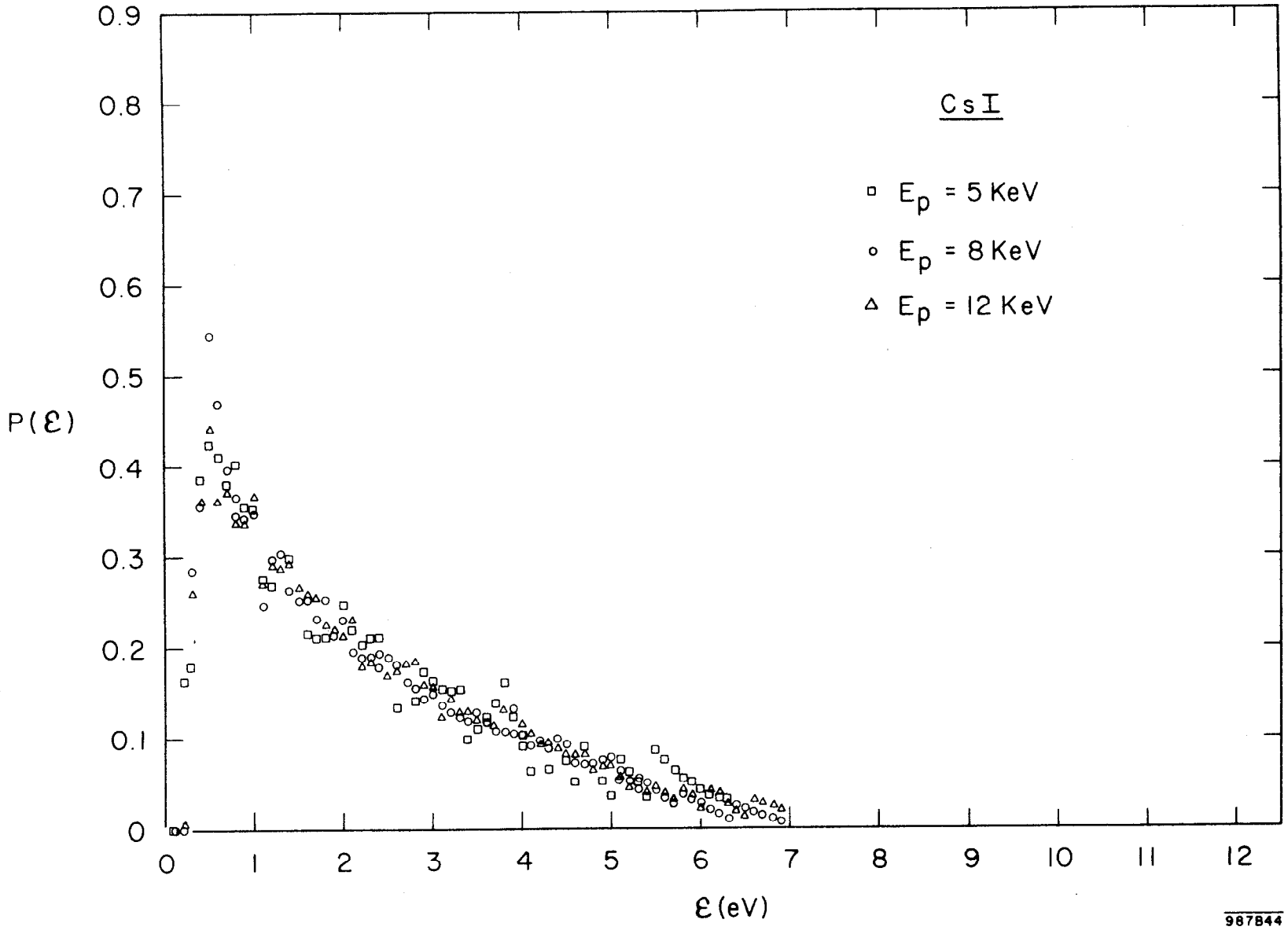
CsI
E_p = 5 KeV
E_p = 8 KeV
E_p = 12 KeV
P(ℰ)
ℰ (eV)
0
0.1
0.2
0.3
0.4
0.5
0.6
0.7
0.8
0.9
0
1
2
3
4
5
6
7
8
9
10
11
12
987844

Fig. 14

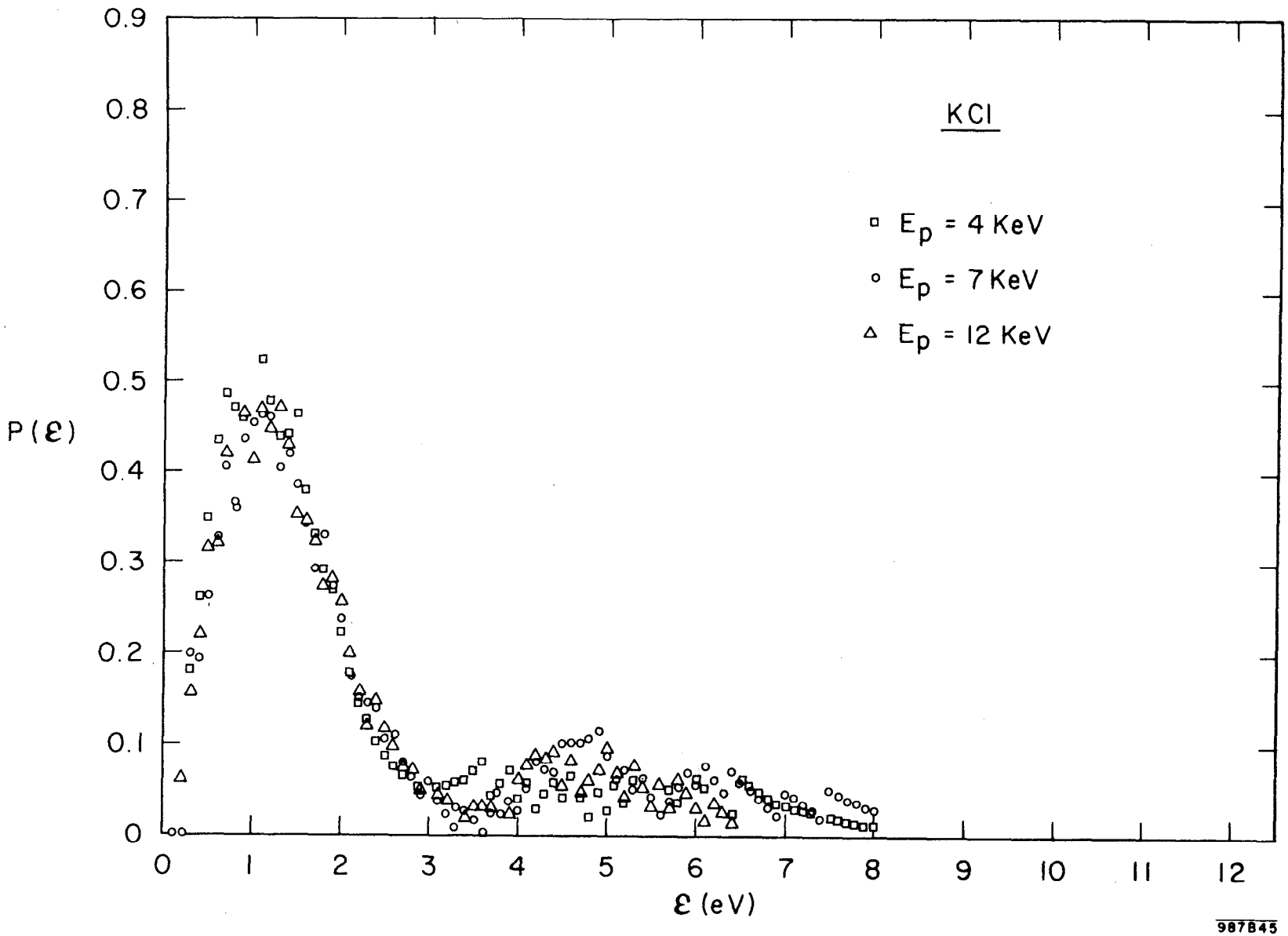
KCl
E_p = 4 KeV
E_p = 7 KeV
E_p = 12 KeV
P(ε)
ε (eV)
0
0.1
0.2
0.3
0.4
0.5
0.6
0.7
0.8
0.9
0
1
2
3
4
5
6
7
8
9
10
11
12
987845

Fig. 15

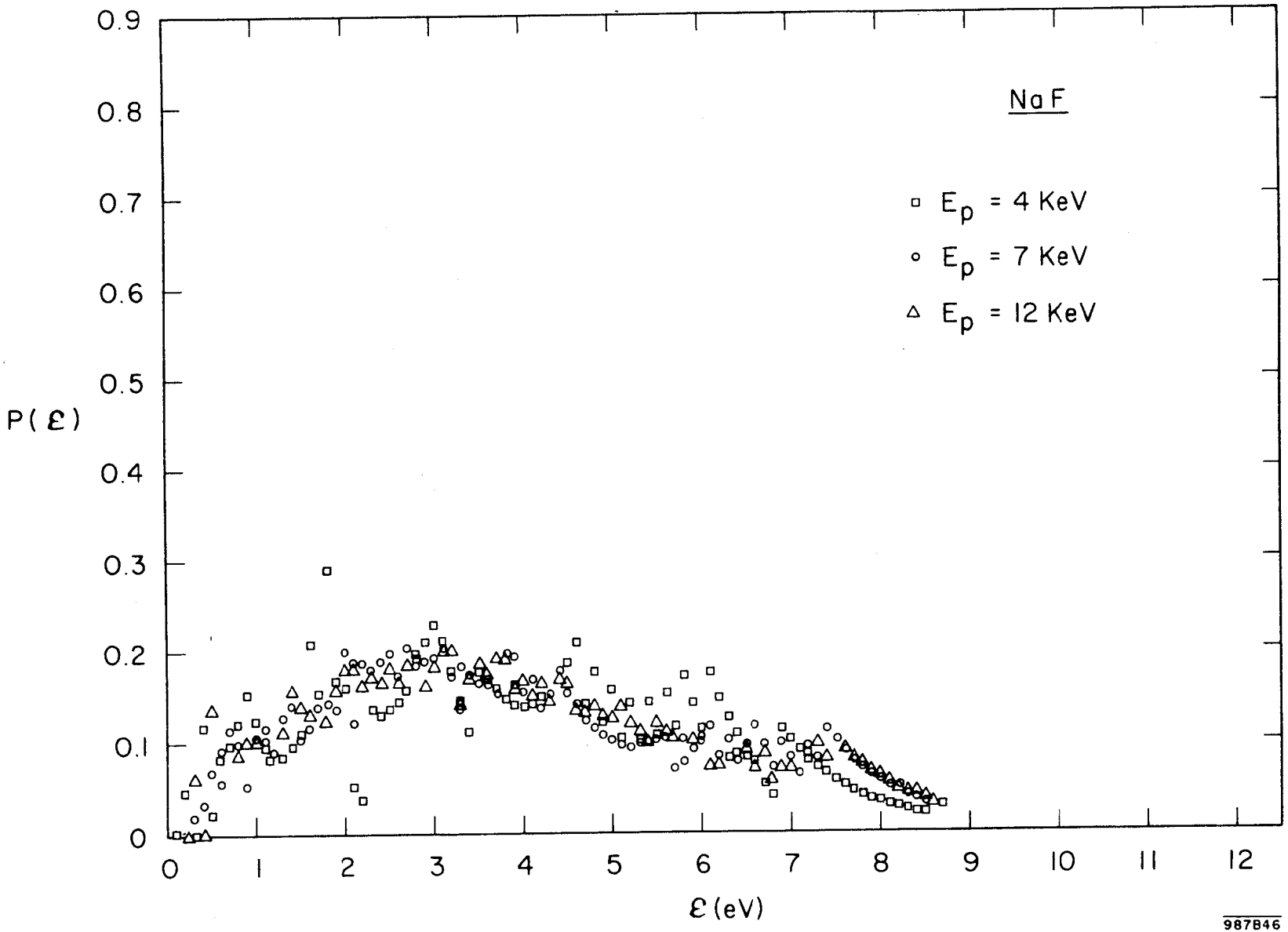
NaF
E_p = 4 KeV
E_p = 7 KeV
E_p = 12 KeV
P(ℰ)
ℰ (eV)
0.9
0.8
0.7
0.6
0.5
0.4
0.3
0.2
0.1
0
0 1 2 3 4 5 6 7 8 9 10 11 12
987B46

Fig. 16

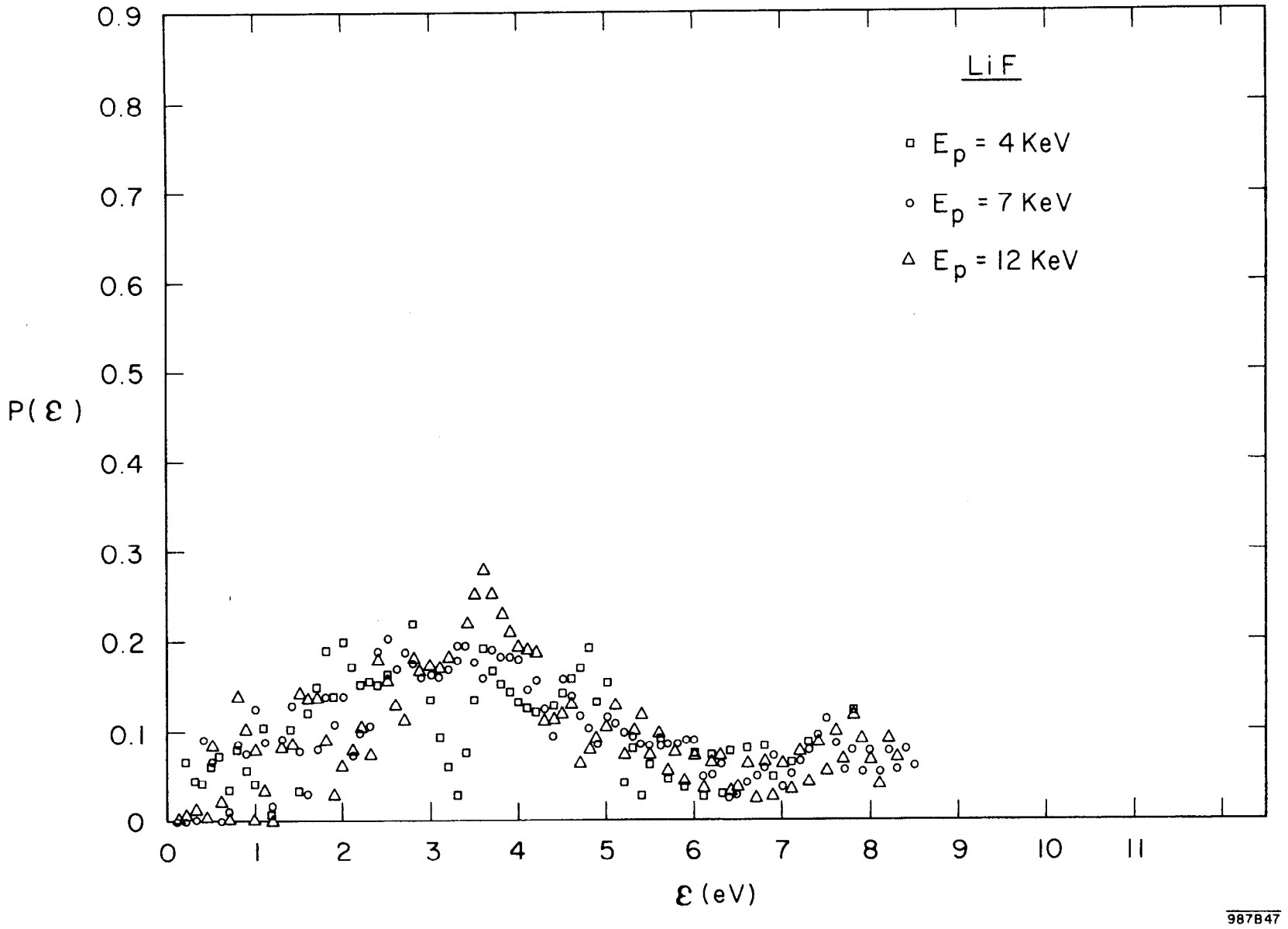
LiF
E_p = 4 KeV
E_p = 7 KeV
E_p = 12 KeV
P(ε)
ε (eV)
0.9
0.8
0.7
0.6
0.5
0.4
0.3
0.2
0.1
0
0 1 2 3 4 5 6 7 8 9 10 11
987B47

Fig. 17

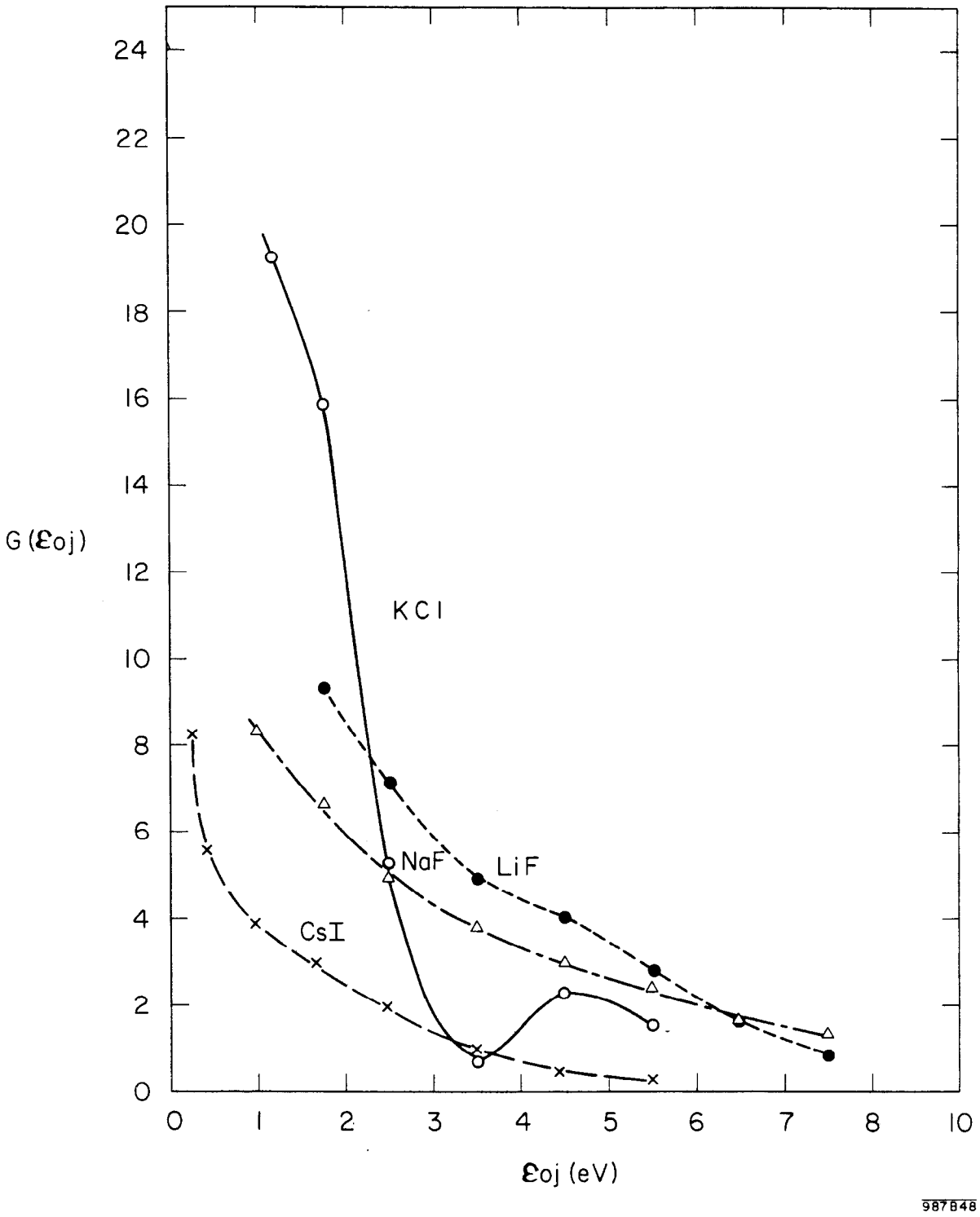
G (ℰoj)
24
22
20
18
16
14
12
10
8
6
4
2
0
0
1
2
3
4
5
6
7
8
10
ℰoj (eV)
KCl
NaF
LiF
CsI
987848

Fig. 18

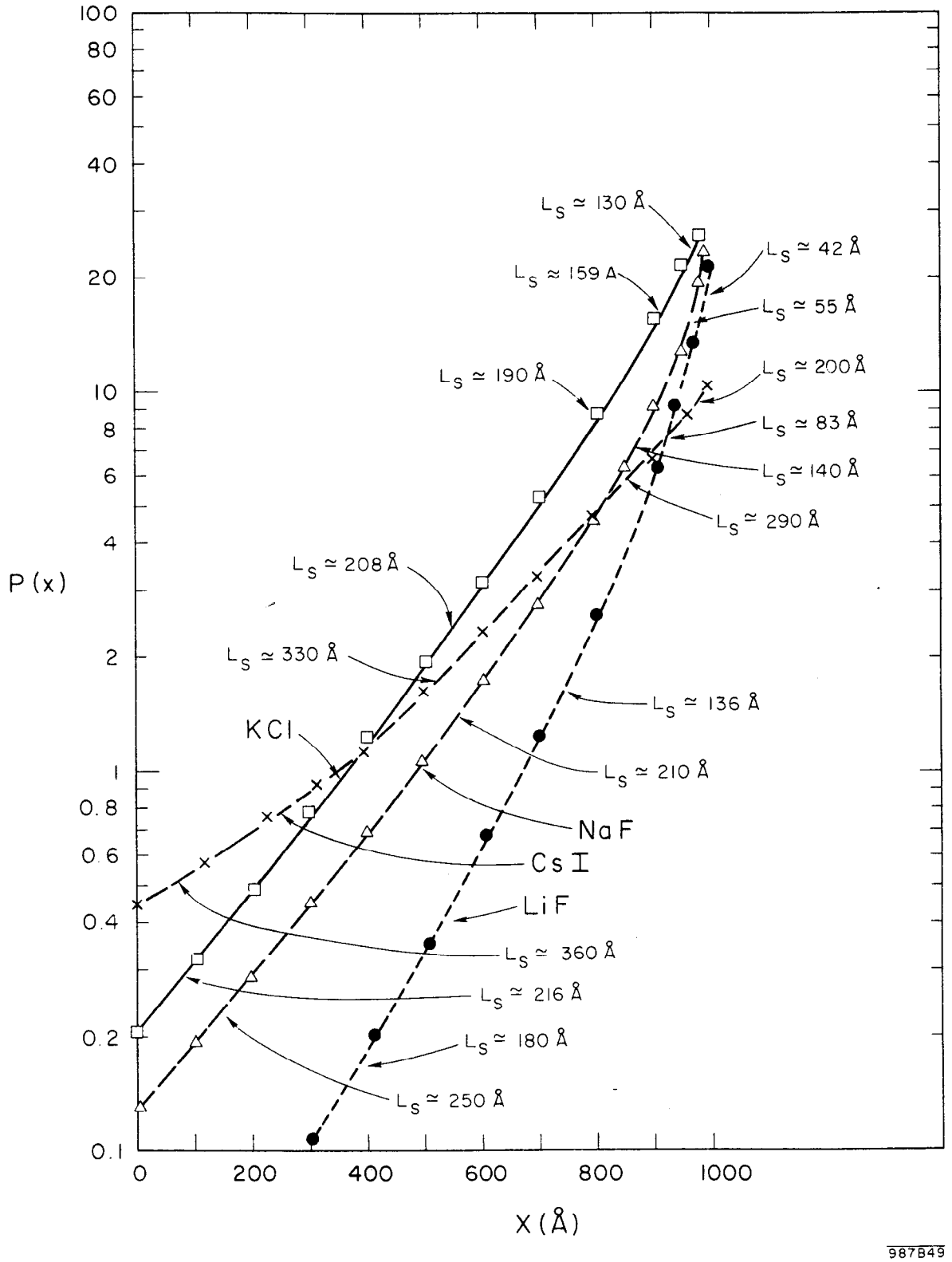
100
80
60
40
20
10
8
6
4
2
1
0.8
0.6
0.4
0.2
0.1
P(x)
0
200
400
600
800
1000
X(Å)
$L_S \simeq 130$ Å
$L_S \simeq 159$ Å
$L_S \simeq 190$ Å
$L_S \simeq 208$ Å
$L_S \simeq 330$ Å
KCl
$L_S \simeq 42$ Å
$L_S \simeq 55$ Å
$L_S \simeq 200$ Å
$L_S \simeq 83$ Å
$L_S \simeq 140$ Å
$L_S \simeq 290$ Å
$L_S \simeq 136$ Å
$L_S \simeq 210$ Å
NaF
CsI
LiF
$L_S \simeq 360$ Å
$L_S \simeq 216$ Å
$L_S \simeq 180$ Å
$L_S \simeq 250$ Å
987B49

Fig. 19